Plasma sheet electromagnetic power generation and its dissipation along auroral field lines

V. Angelopoulos,[1] J. A. Chapman,[1] F. S. Mozer,[1] J. D. Scudder,[2] C. T. Russell,[3] K. Tsuruda,[4] T. Mukai,[4] T. J. Hughes,[5] and K. Yumoto[6]

Received 5 April 2001; revised 5 September 2001; accepted 5 September 2001; published 13 August 2002.

[1] During a fortuitous meridional conjunction of Polar and Geotail at the nightside magnetosphere throughout the course of a geomagnetic substorm, measurements of Poynting flux indicate that most of the electromagnetic energy flux density that is radiated in the form of waves at the location of Geotail at $\sim$18 R_E is dissipated before it reaches Polar at $\sim$5 R_E, i.e., above the auroral acceleration region. While the Poynting flux measured at Polar (and to a greater extent at Geotail) is more than sufficient to account for particle acceleration below the satellite, it still represents a small portion of the earthward directed particle energy flux density measured at Geotail. If even a small portion of the bursty bulk flow energy couples to Alfven waves, it would be energetically sufficient to account for the expected auroral energy deposition during substorms. Power dissipation via kinetic Alfven waves along auroral field lines represents a viable mechanism by which localized reconnection flows can slow down. This may explain why fast earthward flows reported at midtail (>30 R_E) distances can exist with no near-Earth counterpart and why any putative candidates of an ionospherically reflected flow burst pulse in the tail have very small amplitudes. *INDEX TERMS:* 2736 Magnetospheric Physics: Magnetosphere/ionosphere interactions; 2772 Magnetospheric Physics: Plasma waves and instabilities; 2740 Magnetospheric Physics: Magnetospheric configuration and dynamics; *KEYWORDS:* plasma sheet, Poynting flux, ionosphere, Alfven waves, r[transport]

1. Introduction

[2] Recent work [*Wygant et al.*, 2000] suggests that the Poynting flux on auroral field lines at altitudes 4–6 R_E measured by the Polar satellite is at least a factor of 10 larger than expected from measurements of the same quantity at subauroral altitudes. Since the measured electromagnetic energy flux is comparable to the expected particle energy flux in the auroral region, it was surmised that most of the observed electromagnetic energy is actually deposited in the particles within the acceleration region. Such waves represent a significant energy inflow to the auroral ionosphere. The energy source for those waves is expected to be in the tail plasma sheet at or earthward of the neutral line.

[3] Bursty bulk flows (BBFs) represent a significant energy transport toward Earth [*Angelopoulos et al.*, 1994]. Such flows measured on the Active Magnetospheric Particle Tracer Explorer Ion Release Module (AMPTE/IRM) satellite, with apogee at $\sim$19 R_E, correlate statistically with *AL* decreases [*Angelopoulos*, 1996], suggesting that they are an integral part of substorm activity. Exactly how or even how much of this energy gets deposited to the ionosphere is not clear. When studied on a case-by-case basis from close enough to Earth, such flows are indistinguishable from the current disruption process [*Angelopoulos et al.*, 1999], occurring no more than 1 min prior to the earliest substorm onset indicator [e.g., *Angelopoulos et al.*, 1996a]. Much work has been devoted to studying the formation of the current wedge at the interaction of the colliding bursty flow jet with the Earth's dipole [*Shiokawa et al.*, 1997, 1998; *Birn et al.*, 1999]. On fortuitous occasions when multiple magnetospheric and auroral observations were possible during the recovery phase of substorms, fast-flow bursts from the near-Earth tail have been timed to correlate well with geosynchronous injections and simultaneous rapid equatorward motion of auroral luminosity, otherwise known as north-south forms [*Henderson et al.*, 1998; *Sergeev et al.*, 1999]. Such flows can originate as far as 40 R_E from Earth and penetrate through an already dipolarized plasma sheet [*Sergeev et al.*, 2000].

[4] However, fast flows also exist at midtail distances (>30 R_E) in the absence of substorms. Early reports of such midtail flows in the absence of *AE* activity [*Coroniti et al.*,

[1]Space Sciences Laboratory, University of California, Berkeley, California, USA.
[2]Department of Physics and Astronomy, University of Iowa, Iowa City, Iowa, USA.
[3]Institute of Geophysics and Planetary Physics, University of California, Los Angeles, California, USA.
[4]Institute of Space and Astronautical Science, Sagamihara, Kanagawa, Japan.
[5]Herzberg Institute of Astrophysics, National Research Council, Ottawa, Ontario, Canada.
[6]Department of Earth and Planetary Sciences, Kyushu University, Fukuoka, Japan.

0148-0227/02/2001JA900136$09.00

1978, 1980] came from IMP 7. In those cases, plasma heating but no dipolarization or fast flows were seen in the near-Earth environment. A more recent fortuitous Geotail-Wind conjunction [*Oieroset et al.*, 2000] confirmed that such flows can exist in the midtail but not make it in the near-Earth environment, which agrees with the fact that they are not very geoeffective. Such midtail flows have been linked to high-latitude activations [*Lyons et al.*, 1999; *Zesta et al.*, 2000]. Those activations occasionally protrude to lower latitudes and in this sense resemble the north-south arcs, or streamers. When such streamers are initiated at the poleward boundary after the previous development of a "double auroral oval," then a new substorm may erupt at the equatorward boundary [*Elphinstone et al.*, 1995].

[5] It is evident that from the point of view of their ionospheric response, at least three types of bursty bulk flows are present: those that are related to the substorm expansion (pseudobreakups included), those that are related to late substorm recovery (north-south arcs), and those that are related to high-latitude activations. However, from the point of view of local magnetotail flow observations the three types are indistinguishable. Since the occurrence frequency of fast flows increases with distance from Earth [e.g., *Baumjohann et al.*, 1990; *Angelopoulos et al.*, 1994], the midtail flows are interesting because they are so frequent. In particular, the question arises: Where do such flows deposit their (significant) earthward directed energy? Nevertheless, the study of any type of fast flow and its energy dissipation is interesting since, because the three flow types are so similar, it can provide useful information on energy dissipation of all types of fast magnetotail flows.

[6] A broadband spectrum of low-frequency (0.1–10 min) oscillations is present in the flow and electric and magnetic field data. *Sanchez et al.* [1997], using a large array of ground and space observatories, showed that some of the flow periodicity is due to global mode oscillations, while *Kepko and Kivelson* [1999] noted that the observed flow bursty periodicity matches simultaneous Pi2 pulsation peaks. Occasionally, reverse flows are seen a few minutes after an impulsive earthward flow onset, indicating possible ionospheric reflection [e.g., *Angelopoulos et al.*, 1996a, Figure 12; *Angelopoulos et al.*, 1999, Figures 3 and 4]. The occurrence of such tailward flows in the presence of a northward magnetic field has been pointed out more recently by *Schodel et al.* [2001]. Since the nightside ionospheric conductivity is large, an ionospherically reflected pulse is expected to be quite large. In fact, *Nishida* [1979], attempting to explain the presence of tailward flows in the near-Earth tail, showed that the ionospherically reflected pulse can be comparable in magnitude and opposite in direction to the incident pulse. This, however, is contrary to the observation of a smaller reflected pulse in the data. One possibility may be that the reflected pulse in ideal MHD will follow the field line on which it was generated and will not arrive back at the same location as the driver flows. Nevertheless, fast tailward flows are rare in the near-Earth, near-neutral sheet magnetotail, whereas fast earthward flows in the same region are not uncommon [*Baumjohann et al.*, 1990]. Thus the question remains: Why should any evidence of a reflected BBF pulse have so small an amplitude relative to the generating, earthward pulse?

[7] Another related question has to do with the damping rate of the flow. At periods of ~1 min, ionospheric dissipation rates are expected to be quite small, given typical values of Pedersen and Alfven conductivities [e.g., *Lysak and Song*, 1998]. Yet, in reality, BBFs last only a few Alfven bounce periods, i.e., ~10 min relative to an Alfven bounce period of 1–2 min (depending on latitude). If the individual flow bursts are considered [*Angelopoulos et al.*, 1992], then those last as little as 1 min, i.e., barely long enough for the Alfvenic pulse to bounce off of the ionosphere once.

[8] This suggests that an energy dissipation mechanism that does not involve the ionosphere must be present, such that most of the incoming BBF-generated Alfvenic pulse dissipates its energy even before it reaches the auroral ionosphere. In this paper we present further evidence that indeed this is the case, and we link the BBF observations with the aforementioned substorm-time observations of *Wygant et al.* [2000]. In section 2 we present a case study of a fortuitous magnetic conjunction between the Polar and Geotail spacecraft during the course of a substorm. In section 3 we evaluate the electromagnetic energy flux propagating along the field lines at the two spacecraft. We show that in all frequency ranges, there is far more power per unit flux tube radiated toward the ionosphere at the location of Geotail at 18 R_E than is radiated toward the ionosphere at the location of Polar at 5 R_E. We also compare the electromagnetic energy flux in the tail (at Geotail) with the earthward particle energy flux at the same place and find that the latter exceeds the former by a factor of 10. This fact, as well as careful consideration of the components of the electric and flow fields, suggests that the source of the Poynting flux is the east-west motion of the equatorial plasma possibly driven by the interaction of earthward flow bursts with the ambient plasma sheet plasma. Section 4 deals with the **E**-to-**B** ratios of the perturbations associated with the large Poynting fluxes. In section 5 we use particle observations to infer that the regions of peak Poynting flux map in the ionosphere to the region between the polar cap boundary and the active aurorae. In section 6 we summarize our findings, and in section 7 we argue that the dissipation mechanism is probably kinetic Alfven waves launched from the plasma sheet, dissipating much of their energy at or above the altitude of Polar.

2. The Event

[9] We searched for Polar-Geotail meridional conjunctions (foot points within 1.5 magnetic local time (MLT) hours) in the period from March 1, 1996, to May 31, 1997, at the nightside (between 2100 and 0300 MLT) and found 46 conjunction events. During only one of those conjunctions did a substorm occur close enough in space (i.e., in local time) and in time such that both spacecraft experienced the anticipated magnetic and electric field variability associated with substorms [e.g., *Keiling et al.*, 2000; *Nagai et al.*, 1998]. This event occurred on November 13, 1996, between 0900 and 1200 UT. Figure 1 presents the equatorial (International Geomagnetic Reference Field mapping to magnetic equator) and meridional (GSM) projections of the spacecraft. Polar was in an outbound leg of its orbit moving from below to above the magnetic equator, essen-

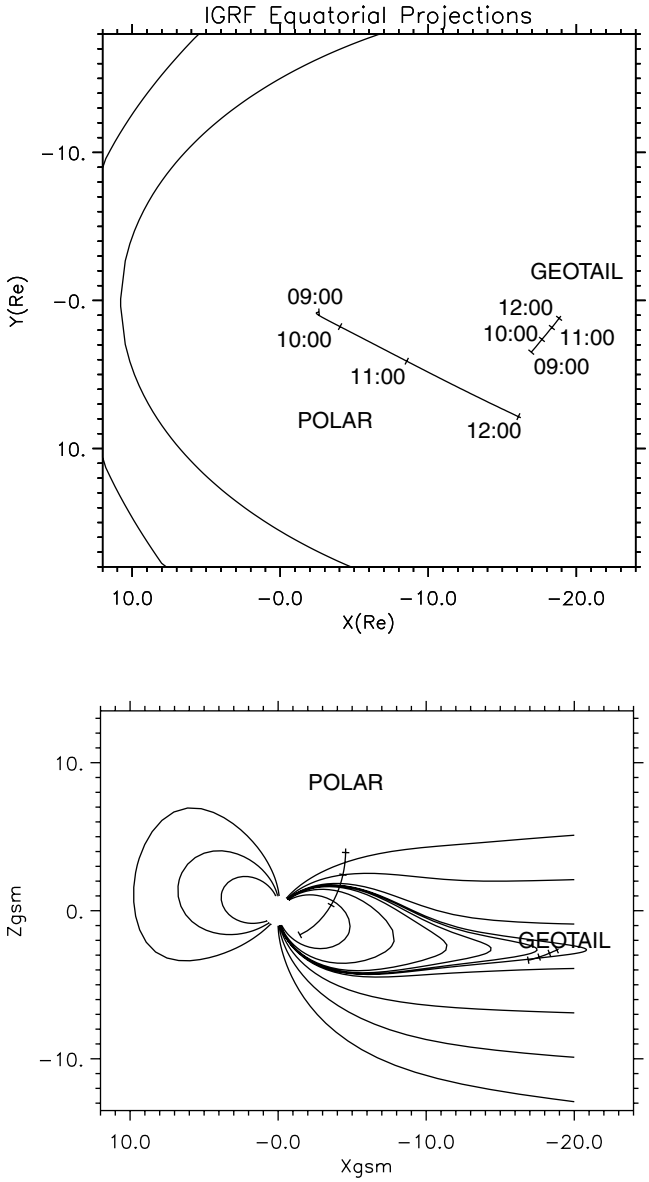

Figure 1. (top) Equatorial projections of Polar and Geotail spacecraft during the interval 0900–1200 UT on November 13, 1996, using the International Geomagnetic Reference Field model. (bottom) X–Z GSM projections of the same spacecraft along with projections of magnetic field lines from the T89 [*Tsyganenko*, 1989] model having equatorial foot points in the noon–midnight meridian. Tick marks are every hour.

tially along the 22.3 MLT meridian, while increasing in radial distance from 3.9 to 6.4 R_E. Geotail was in the tail; its equatorial projection was moving more slowly than Polar's in the eastward and tailward direction. The equatorial footprints of the two spacecraft were along the Sun-Earth line at ~1020 UT.

[10] Figure 2 presents the ionospheric footprints of the spacecraft using the *Tsyganenko* [1989] model (hereinafter called the T89 model) along with the anticipated oval location for the measured *AL* [*Feldstein and Starkov*, 1967; *Starkov*, 1994]. The snapshot of the Earth and a superimposed corrected geomagnetic coordinate grid are shown for 1030 UT. Tick marks along the satellite footprints are every hour (same as in Figure 1); the arrow shows the direction of motion in geographic coordinates. The MLT separation of the ionospheric footprints varies from ~0.5 hours at 0900 UT to ~1.5 hours at 1200 UT.

[11] While no space imager data was available at the time, the ground-based meridional scanning photometer at Poker Flat was operating (Poker Flat was located between the Geotail and Polar foot points at 1020 UT, though much closer to Geotail). The photometer data from Poker Flat are shown in Figure 3. The 5577A data show the discrete auroral emissions and show evidence for a substorm precursor at 0932 UT (no significant poleward development), at 1018 UT (onset), and 1038 UT (major intensification).

[12] The northward component (X) data from auroral latitude ground magnetometer stations (whose positions were indicated in Figure 2) are shown in Figure 4. On the basis of the magnitude of the perturbations it is evident that the main substorm activity was seen near the Alaskan sector. A second substorm took place at 1310 UT over the Russian sector, but that is unrelated to our study.

[13] The northward (X) and eastward (Y) component data from midlatitude ground stations are shown in Figure 5. Note that EWA (Ewa Beach) was at 23.9 MLT, while GAM (Guam) was at 20.3 MLT at 1030 UT. The positive excursion seen in the X components at ~1038 UT confirms the global nature of the main substorm intensification. The opposite sign excursion in the Y component data shows that the substorm meridian was between the two stations at 1038 UT.

[14] Polar observations are summarized in Figure 6 for the period 1000–1200 UT. The top panel shows the reverse of the spacecraft potential (SCPOT), which corresponds (in a nonlinear but monotonic fashion) to the ambient plasma density, measured by the Electric Field Instrument (EFI)

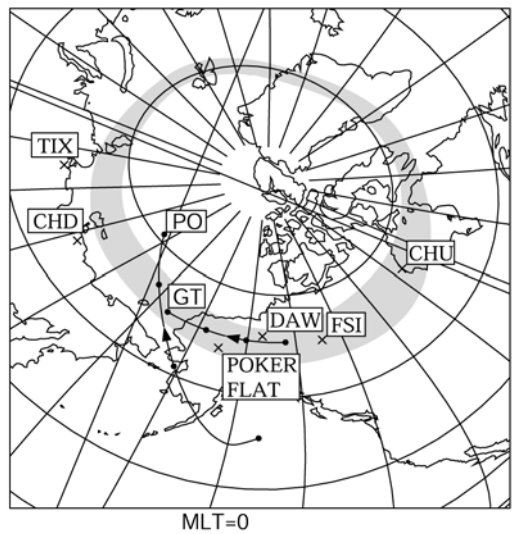

Figure 2. Ionospheric magnetic footprints of Polar and Geotail using the T89 model and shown in geographic coordinates. The snapshot of Earth is shown at 1030 UT. A corrected geomagnetic coordinate system is superimposed on the globe for the same time. Superimposed also is the *Feldstein and Starkov* [1967] auroral model for the activity level at the time [*Starkov*, 1994].

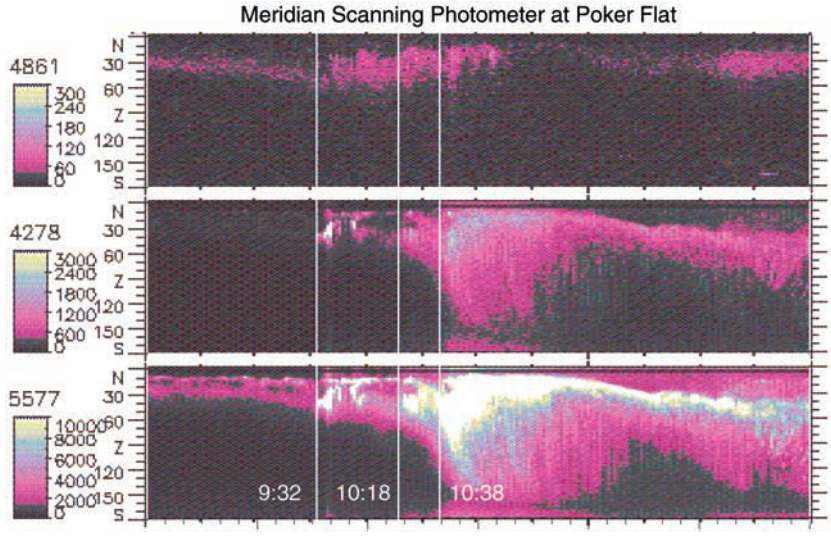

Figure 3. Data from the meridional scanning photometer at Poker Flat (location shown in Figure 2). Vertical lines denote a substorm precursor, the onset, and a major intensification.

[*Harvey et al.*, 1995]. At 1000 UT the spacecraft was in the plasmasphere, as evidenced by the large value of SCPOT. Exit from the plasmasphere occurred at ~1020 UT, possibly in response to the substorm onset. Plasma sheet/lobe densities ($0.01-1$ cm^{-3}) are consistent with the SCPOT values thereafter.

[15] The magnetic and electric field data from the Magnetic Field Experiment (MFE) instrument [*Russell et al.*, 1995] and the EFI on Polar are shown in the *X-Y, Z*, 56-coordinate system at spin-period (6 s) resolution. The unit vectors **X-Y** and **Z** are on the satellite spin plane, with **X-Y** opposite to the projection of the satellite-sun vector on the spin plane and with **Z** normal to the *X-Y* axis, positive closest to the north. The unit vector 56 is along the spin axis in the direction such that *X-Y, Z*, and 56 form an orthogonal basis. The directions of *X-Y* and 56 depend on the time of

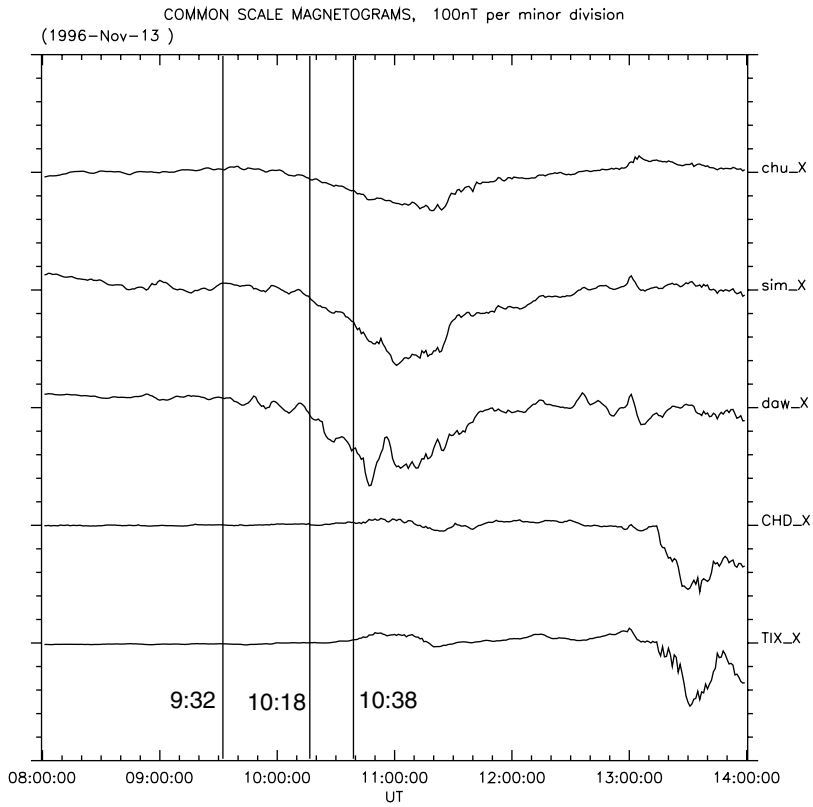

Figure 4. Auroral zone common-scale ground magnetograms from stations shown in Figure 2. Each minor tick mark is 100 nT.

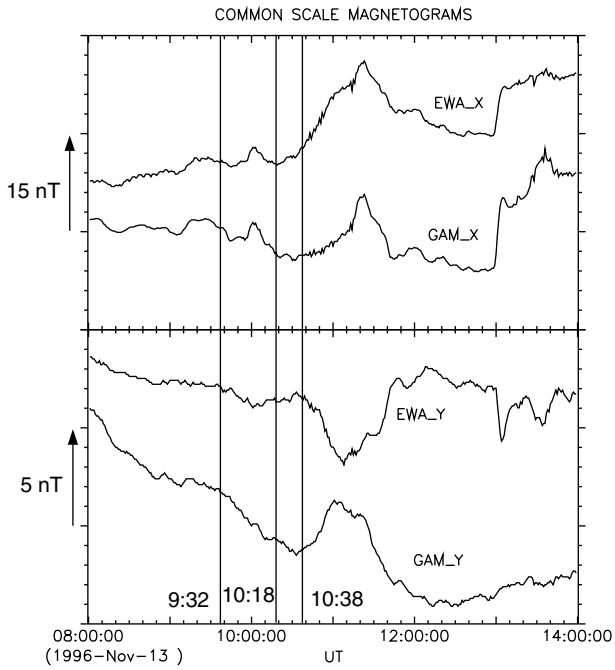

Figure 5. Midlatitude, common-scale ground magnetograms in the north-south (*X*, positive north) and east-west (*Y*, positive east) directions.

the year but are independent of the satellite spin flips that occur twice a year. For the event under study, *X*-*Y* points roughly opposite to X_{GSE}, while 56 points roughly duskward. The large variability in the electric field data is an indication of traversal of the (high beta) plasma sheet; exit from the plasma sheet is demarcated by the reduction in such low-frequency fluctuations at ~1135 UT.

[16] Geotail observations for the same period (1000–1200 UT) are summarized in Figure 7. Magnetic field and plasma data are plotted at 12-s resolution in GSM coordinates. The electric field can be computed at the same (12 s) resolution from the plasma approximation, $\mathbf{E} = -\mathbf{V} \times \mathbf{B}$; its components are plotted as solid lines in GSE coordinates in the bottom three panels. Electric field data are also directly measured by the electric field experiment (EFD) and are plotted on the same panels as dots at spin-period (3 s) resolution. The EFD instrument measures the electric field between the tips of a spinning antenna, and spin fits of that (one dimensional) measurement are used to obtain the *X* and *Y* spin plane (near-GSE) components. The third component (E_Z) can be computed only when the magnetic field is sufficiently away (by more than ~10°) from the spin plane. At the times that this condition is met, this computation was performed; the points are presented also as dots in the bottom panel. Typically, the electric field measured by the EFD instrument agrees quite well with the electric field inferred from the plasma data, except at low flow velocities where the diamagnetic drifts (~10 km s^{-1}) start becoming important. At times of fast flows the electric field data at 3-s resolution measured by the EFD instrument are much more variable than the 12-s averages computed from the plasma data, indicating an increased level of wave power that is not fully resolved at 12-s resolution.

[17] Prior to 1000 UT, Geotail showed multiple traversals of the magnetic equator without significant flows or magnetic noise. Geotail exited to the lobe, as evidenced by the decrease in density and temperature at 1020–1024 UT, and reentered in an "active" plasma sheet, i.e., a plasma sheet accompanied by fast earthward flows at the boundary layer and neutral sheet. The boundary layer flows at 1022–1026 UT are typical of this situation, which has been termed "plasma sheet recovery." The ensuing neutral sheet flows are typical of the bursty bulk flows studied previously [e.g., *Angelopoulos et al.*, 1996a]. The plasma sheet dipolarized at 1115 UT. Some bursty bulk flows are seen also during that dipolarization, which is expected to map at high latitudes in the auroral oval. Fast-flow activity ceased at 1130 UT at Geotail, and the plasma sheet thinned at 1140 UT (evidenced by the reduction of $\mathbf{B}_Z$ to the value that it had prior to substorm onset, or a few nT). Cessation of activity at Geotail corresponds to completion of substorm recovery as evidenced by auroral zone magnetograms. The entire interval of fast-flow activity at Geotail is accompanied by large-amplitude fluctuations in the electric and magnetic fields.

[18] The entry of Polar in the plasma sheet at 1018 UT and the exit of Geotail from the plasma sheet at around the same time are most likely related to the onset of the substorm. The working phenomenological hypothesis is that the plasma sheet reconnects underneath or slightly earthward of Geotail and the inner edge of the plasma sheet moves earthward as a result of the associated reconnection flows. The exit of Polar from the plasma sheet at ~1135 UT and the plasma sheet thinning at Geotail at 1140 UT are most likely related to the completion of the substorm recovery. The plasma sheet thinned again as part of a growth phase of a subsequent substorm that occurred at 1310 UT.

[19] Evidently, Polar's and Geotail's large-scale motions relative to distinct magnetotail regions are consistent with the substorm which occurred and consistent with each other, in accordance with their approximate alignment along the Sun-Earth direction. The large amplitude and variability of electric fields observed simultaneously at the two spacecraft are also consistent with each other. These facts suggest that the two spacecraft not only have nearby model ionospheric projections but that they were traversing flux tubes undergoing similar processes. This is ultimately why this event was chosen as a good candidate to check mapping of electromagnetic energy from high to low altitudes.

3. Energy Flux

[20] In this section we compare the energy flux density measured on Geotail and Polar. Figure 8 shows the most variable of the three components of the electric field on Polar (dE_Z) and the associated magnetic field component ($d\mathbf{B}_{56}$) after high-pass filtering components $\mathbf{E}_Z$ and $\mathbf{B}_{56}$ of Figure 6 through subtraction of a running average with a 10-min window. After forming the Poynting flux in the *X*-*Y*, *Z*, 56 system, we obtain its field-aligned component by dotting it with the unit magnetic field vector obtained after averaging the magnetic field data with a 10-min-window running average. The resultant parallel Poynting flux in units of ergs cm^{-2} s^{-1} is plotted in the top panel of Figure 8 (SPAR).

[21] One caveat here is that the E_{56} component used in the computation of SPAR requires offset corrections that are

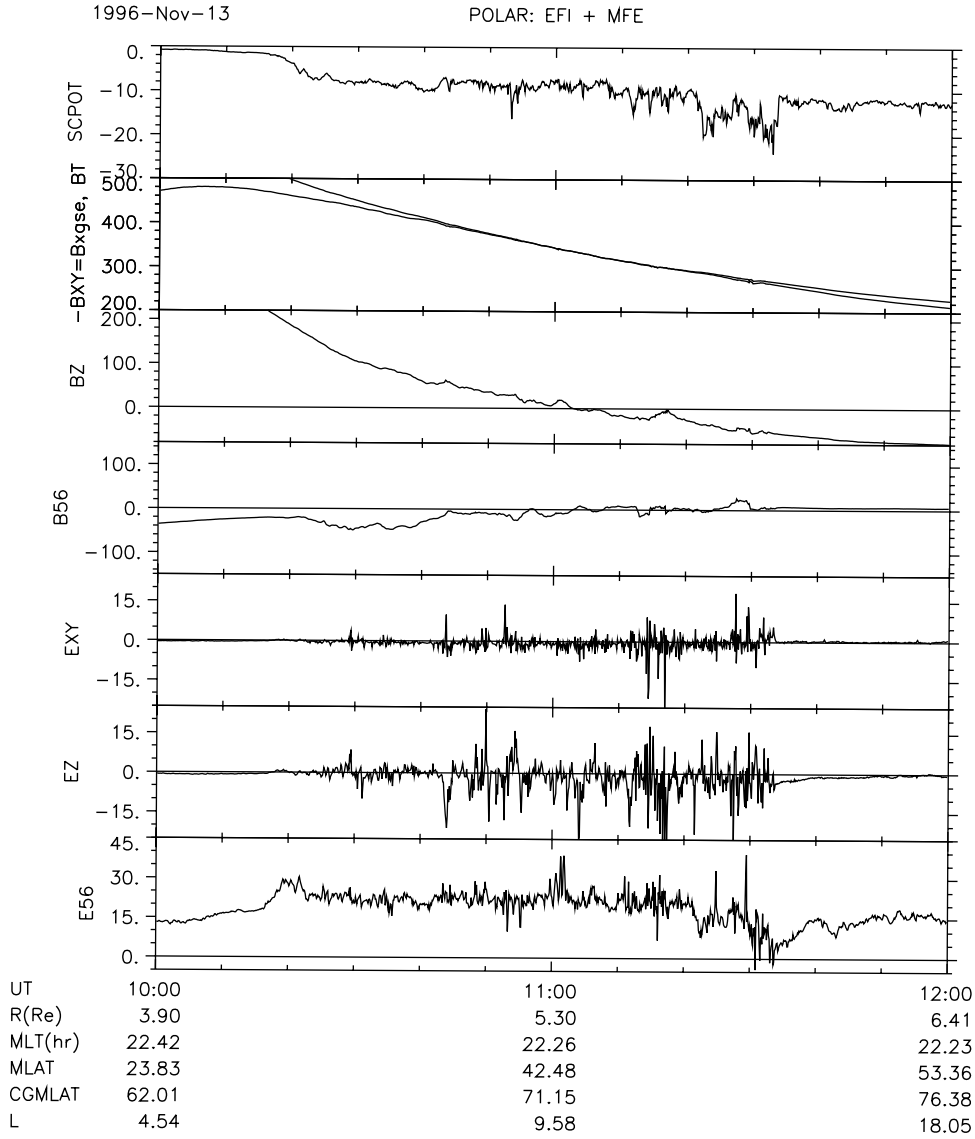

Figure 6. Event overview from the Polar spacecraft at spin-period resolution (6 s).

nontrivial. The offsets depend on the ambient density (and less so on the electron temperature), as inferred from an examination of long periods of data from several orbits and as suggested by the correlation of E_{56} and SCPOT (proxy for plasma density) during the two SCPOT drops between 1120 and 1135 UT in Figure 6. However, we are interested only in the high-frequency part of the fluctuations in the computation of SPAR, which is least affected by such offset uncertainties. To verify the behavior of SPAR we also computed the E_{56} component under the assumption that $\mathbf{E} \cdot \mathbf{B} = 0$ and used it to recompute the parallel Poynting flux. This is denoted $SPAR_0$ and is also plotted in Figure 8. The computation of E_{56} can be done safely when the magnetic field is sufficiently away from the spin plane or when $\mathbf{B}_{56}$ is no less than 15% of the total field value. The $SPAR_0$ component in Figure 8 compares quite favorably with the SPAR component, which gives credence to our assumption that offset corrections for the high-pass filtered E_{56} are negligible.

[22] It is evident that the Poynting flux is directed along the field line (toward Earth) and that although a low-frequency oscillation dominates the magnetic field fluctuations, the Poynting flux is composed of pulses no longer than a couple of minutes in duration. These are very similar to attributes of the computed Poynting flux at that altitude as described by *Wygant et al.* [2000]. What is different from the events described by Wygant et al. is the amplitude of the electric, magnetic, and Poynting flux pulses, which are a factor of 5 smaller here than in the substorm events selected by Wygant et al. This is not due to the activity (*AL* was approximately −100 nT for one and −1500 nT for the other of the two Wygant et al. events, while our event occurred during intermediate negative bay magnitudes of ∼400 nT). Rather, it is most likely due to the selection by Wygant et al. of the largest electric field events in the course of a year (1997). The large magnitude of the Wygant et al. events may have to do with the fact that their crossings are both inbound. Typically, an active time plasma sheet boundary is crossed when the boundary moves past the spacecraft. Near substorm onset the inner magnetosphere is compressed, which typically brings the plasma sheet boundary inward.

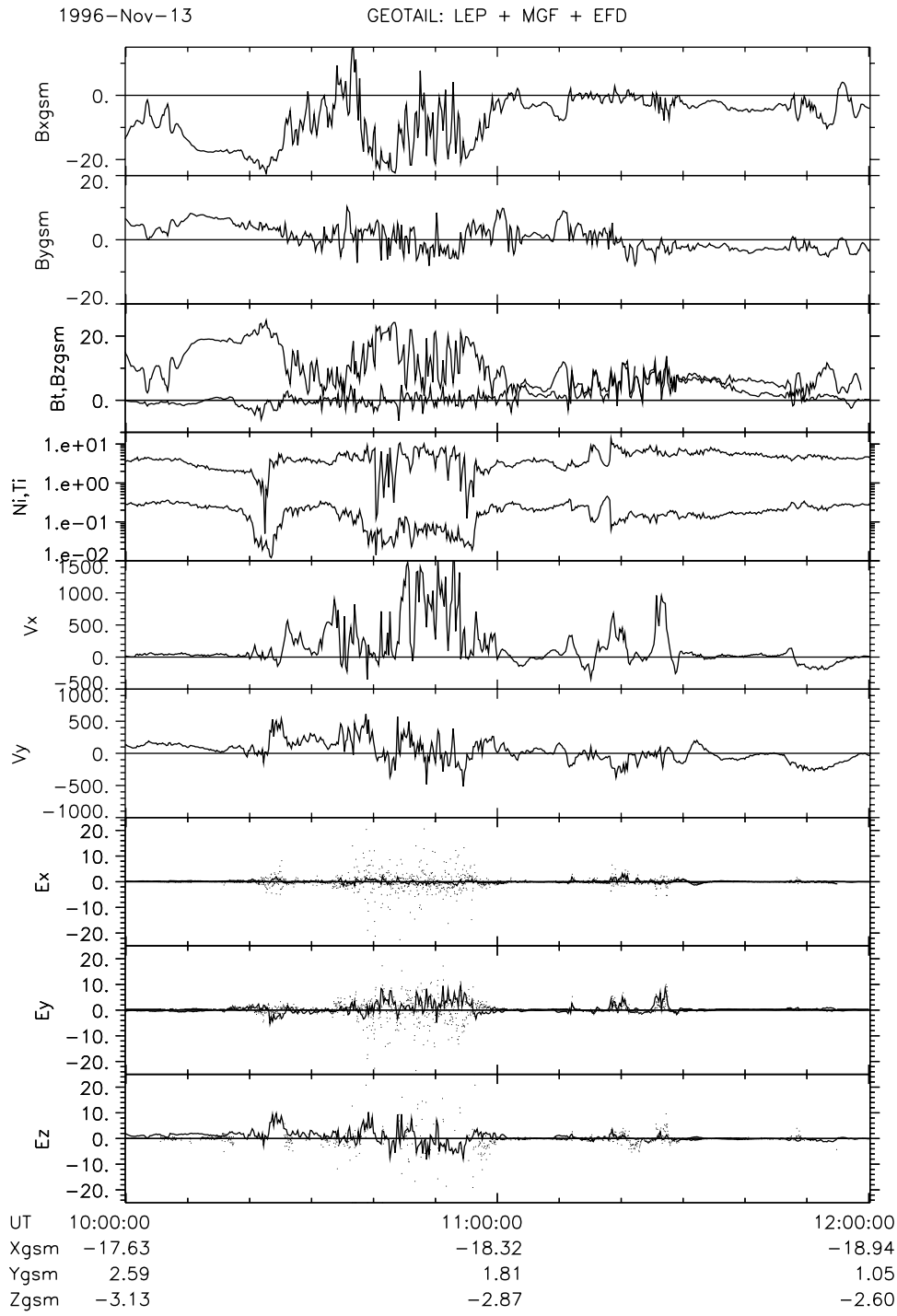

Figure 7. Event overview from the Geotail spacecraft. The resolution is 12 s for the magnetic field **B** (nT) and the plasma flow **V** (km s^{-1}), density N_i (cm^3) and temperature T_i (keV) data and 3 s for the electric field **E** (mV m^{-1}) data.

An inbound orbit remains longer at the plasma sheet boundary and can resolve spatial structures at the 6-s spin-period resolution better than an outbound orbit.

[23] Testimony to that interpretation is the fact that when high time resolution (40 points/s) data are used, then the peak absolute amplitude of the oscillations for our event is comparable to the peak absolute amplitude of the events of *Wygant et al.* [2000] (i.e., ~200 mV m^{-1}). This is shown in Figure 9 for a subset of the data near the plasma sheet boundary layer. In Figure 9 the three components (*X-Y*, *Z*, and 56) of both the electric and magnetic fields are plotted in dashed lines. Solid lines represent the data rotated in the coordinate system *ijk* determined from the principal axes of the electric field variance matrix. The maximum variance axis *i* is closest to the Z direction, the minimum variance axis *k* is nearly aligned with the *X-Y* direction (as expected, since $\mathbf{E} \cdot \mathbf{B} = 0$ to within experimental uncertainties and $\mathbf{B}_{XY}$ is the dominant magnetic field component), and the

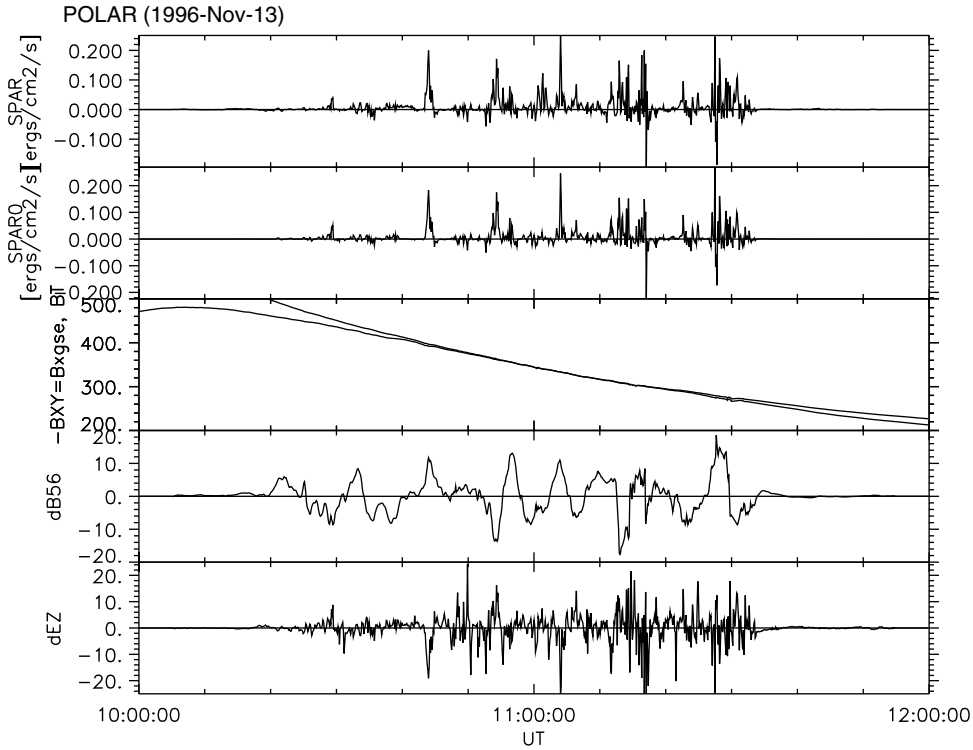

Figure 8. Quantities derived from the Polar data of Figure 6, except for $\mathbf{B}_{XY}$ and $\mathbf{B}_T$, which are the same as in Figure 6. The $d\mathbf{E}_Z$ and $d\mathbf{B}_{56}$ are detrended electric and magnetic field data derived from $\mathbf{E}_Z$ and $\mathbf{B}_{56}$ after subtracting a 10-min running average. SPAR is the Poynting flux computed from such detrended traces of the full **E** and **B** vectors and projected along the instantaneous magnetic field direction. $SPAR_0$ is the Poynting flux computed by using only the spin-plane components of the electric field and assuming $\mathbf{E} \cdot \mathbf{B} = 0$ to obtain the third component.

intermediate variance axis *j* is closest to the 56 direction (duskward). An angle of 30° exists between the *i* and the *z* directions. Assuming that the magnetic fluctuations are due to crossings of field-aligned current sheets aligned with the plasma sheet boundary surface, this angle denotes the angle between the plasma sheet boundary normal and the Z_{GSE} axis. The value of 30° is quite reasonable given the large undulations of the plasma sheet boundary surface that have been reported during substorms using other techniques [*Kettmann and Daly*, 1988]. Note that the coordinate system chosen is nearly identical to the coordinate system that can be obtained from the principal axes of the magnetic variance matrix. It is also noteworthy that in both systems the parallel component of the electric field is consistent with zero.

[24] The low-frequency (spin resolution) peak Poynting flux (from Figure 8) is 0.25 ergs cm^{-2} s^{-1}, which, when mapped to the auroral ionosphere with a mapping factor of 125 (ratio of ionospheric and local values of magnetic field is ~50,000/400 nT = 125), gives 31 ergs cm^{-2} s^{-1}. The full-resolution (40 points/s) data peak Poynting flux (from Figure 9) is 1.25 ergs cm^{-2} s^{-1} and occurred in an ambient field of 280 nT. When the appropriate mapping factor (50,000 / 280 nT = 178) is used, the ionospheric equivalent is ~220 ergs cm^{-2} s^{-1}, i.e., comparable to the largest events selected by Wygant et al. This energy flux is ~2 orders of magnitude larger than the typical fluxes seen below the auroral acceleration region [*Kelley et al.*, 1991].

[25] The largest fluxes of downgoing electrons seen at Defense Meteorological Satellite Program (DMSP) altitudes (800 km) have energy flux density of 100 ergs cm^{-2} s^{-1} [e.g., *Newell*, 2000], which, when mapped to a 100-km reference altitude, correspond to 136 ergs cm^{-2} s^{-1}. Thus the high-resolution Poynting flux measured at Polar can account for even the highest measured energy fluxes of accelerated electrons measured below the acceleration region on auroral field lines by DMSP. As argued by *Wygant et al.* [2000], the upward secondary electrons do not exceed 25 ergs cm^{-2} s^{-1} within arcs [*Stenbaek-Nielsen et al.*, 1998], while upflowing ion energy flux mapped to 100 km altitude is only a fraction (a few percent) of the energy of the downgoing electrons within arcs [*Ghielmetti et al.*, 1979]. Even at the poleward boundary, where such ion outflow fluxes maximize [*Carlson et al.*, 2000], and even at storm times, the largest energy fluxes are on the order of 10 ergs cm^{-2} s^{-1} when mapped to 100 km altitude [*McFadden et al.*, 2001]. Therefore the Poynting flux observed during our event can account for the energy deposited in the particles in the auroral acceleration region. This conclusion is in agreement with the findings of Wygant et al.

[26] The presence of Geotail on the same meridian as Polar readily provides a measure of the energy flux available at that distance. Figure 10 shows computations of the Poynting and the particle energy flux at Geotail. The Poynting flux is computed two ways: using the electric field measured by the EFD instrument (3-s resolution) and

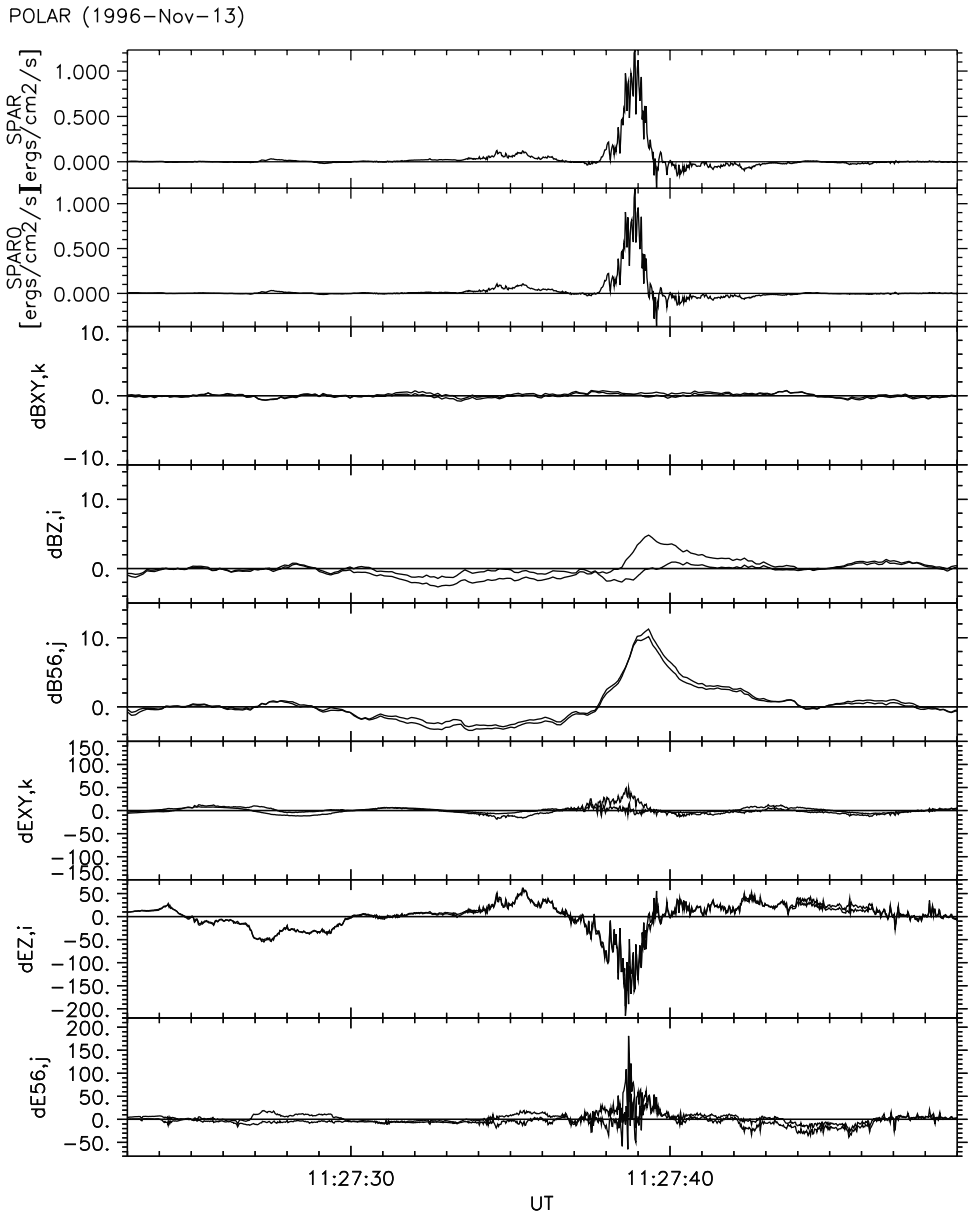

Figure 9. SPAR and $SPAR_0$, the same quantities as in Figure 8, except computed from high time resolution data (0.025 s for **E** and 0.12 s for **B**). The window used for running average subtraction was 20 s. Dashed lines represent data in the *X*-*Y*, *Z*, and 56 coordinate system. Solid lines represent data in the coordinate system *ijk* obtained from minimum variance analysis on the electric field. This is nearly identical to the principal axes directions obtained from performing a minimum variance analysis on the magnetic field.

using the electric field computed from the plasma approximation (12-s resolution). E_Z is the largest of the three components of the computed electric field, as evidenced in Figure 7. Since E_Z is not measured by the EFD instrument but is a quantity derivable only when the magnetic field is favorably oriented (away from the spin plane), E_Z is not available at 3-s resolution all the time. Instead of using incomplete data we obtained the three components of the perpendicular electric field assuming the electric field was all in the *X*-*Y* plane. This is an underestimate of the full electric field. The perpendicular component of the EFD-measured electric field in the *Z* direction is nonzero but small (i.e., mostly immeasurable) and is shown as dots in the bottom panel of Figure 10, along with E_Z computed from the plasma data at 12-s resolution (solid line). We subtracted a 10-min-window running average from both the magnetic field and plasma data (two bottom panels) before computing the Poynting flux.

[27] As mentioned earlier, $dE_Z \times dB_Y$ is the largest contributor to the parallel Poynting flux at Geotail. As evidenced by Figure 7, $\mathbf{E}_Y$ is the largest contributor to the cumulative (earthward) magnetic flux transport because of its nonzero average value over the event, yet the fluctuation amplitude in $\mathbf{E}_Z$ is larger than that of $\mathbf{E}_Y$ (and far greater than

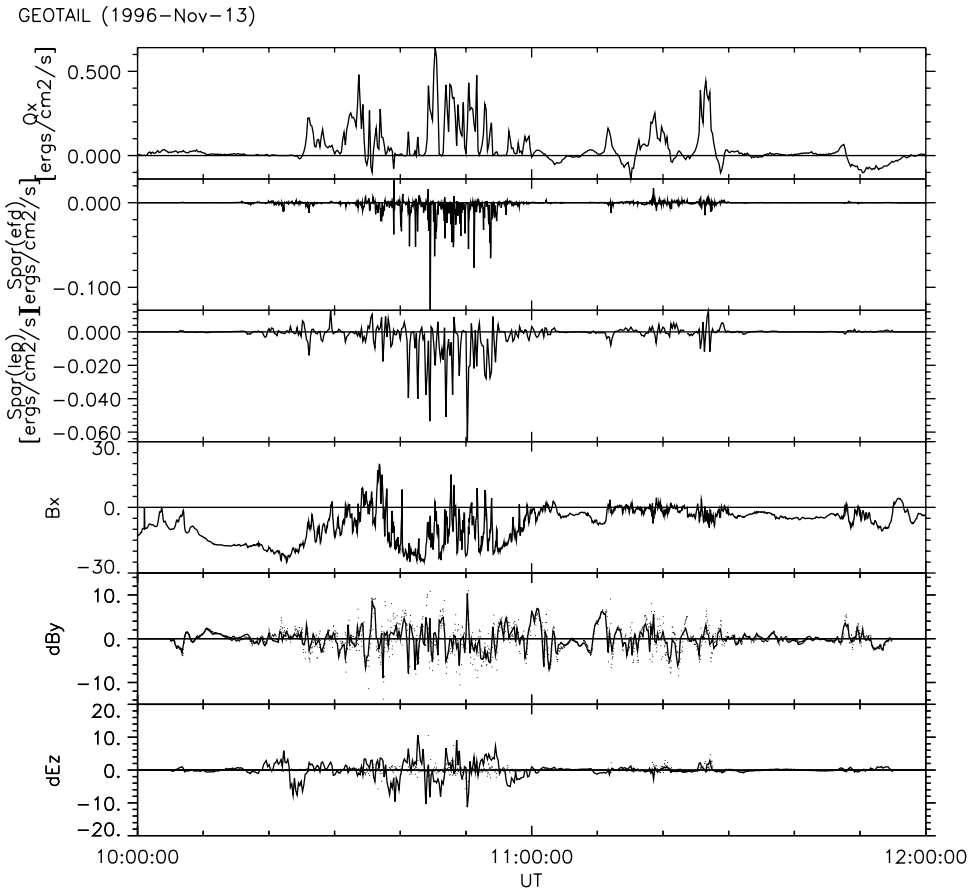

Figure 10. Quantities derived from the Geotail data of Figure 7, except for $\mathbf{B}_X$, which is the same as in Figure 7. The $d\mathbf{E}_Z$ and $d\mathbf{B}_Y$ are detrended electric and magnetic field data derived from $\mathbf{E}_Z$ and $\mathbf{B}_{56}$ after subtracting a 10-min running average. SPAR(lep) is the field-aligned component of the Poynting flux computed from the full **E** and **B** data, where the electric field was obtained from the measured plasma flow assuming the $\mathbf{E} = -\mathbf{V} \times \mathbf{B}$ approximation. This is at 12 s resolution. SPAR(efd) is the Poynting flux computed from the electric field measured by the EFD instrument assuming $\mathbf{E}_Z = 0$ at 3-s resolution. It is an underestimate of the actual value of SPAR. Q_X is the earthward MHD energy flux computed at 12-s resolution from plasma and magnetic field data.

that of $\mathbf{E}_X$) at Geotail. The similarity of the trace of $\mathbf{E}_Z$ to V_Y shows that the term $-V_Y \times B_X$ is the most important contributor to the $\mathbf{E}_Z$ fluctuations and, consequently, to the Poynting flux. These dawn-dusk flows have been noted before [e.g., *Angelopoulos et al.*, 1994], but they do not contribute significantly to a net transport. Their average over many bursty flow events is a small duskward component consistent with diamagnetic drifts of particles measured by plasma instruments (though having no electric field signature). According to our observations these $\mathbf{V}_Y$ flows are the origin of the field-aligned Poynting flux measured at Geotail.

[28] The Poynting flux component parallel to the magnetic field, SPAR, points predominantly opposite to the field direction; since Geotail was below the neutral sheet, this means the flux was directed away from the neutral sheet and into the ionosphere. The peak Poynting flux is on the order of 0.1 ergs cm^{-2} s^{-1} at a resolution of 3–12 s. When mapped to the ionosphere (mapping factor of ~50,000/20 = 2500), it corresponds to 250 ergs cm^{-2} s^{-1}, i.e., approximately an order of magnitude larger than the value computed earlier from Polar at a similar time resolution (31 ergs cm^{-2} s^{-1} at 6-s resolution). Despite the fact that the SPAR computed at 3-s resolution from the perpendicular component of the 2-dimensional (2-D) electric field data is an underestimate of the true value of SPAR, its peak value is larger than the peak value of SPAR computed from the plasma data at 12-s resolution. This means that (much like in the case of Polar) higher-frequency data could result in even higher Poynting flux peak values.

[29] Since the EFD instrument is a single-axis measurement of the electric field, it is not possible to obtain routinely the three components of the electric field. However, the projection of the instantaneously measured electric field along the X and Y axes and the approximation that $\mathbf{E}_Z = 0$ can result in a proxy of the real electric field. When the perpendicular component of that is considered (i.e., **E** parallel is ignored), the resultant parallel Poynting flux measurement is a lower limit of the actual parallel Poynting flux. The problem with this method is that it ignores the $\mathbf{E}_Z$ variation, which, according to the electric field values as computed from the plasma data, may be the dominant one (see Figure 7). To amend this deficiency completely is impossible with a 1-D measurement that is always obtained normal to the direction of interest (Z). A way to occasionally

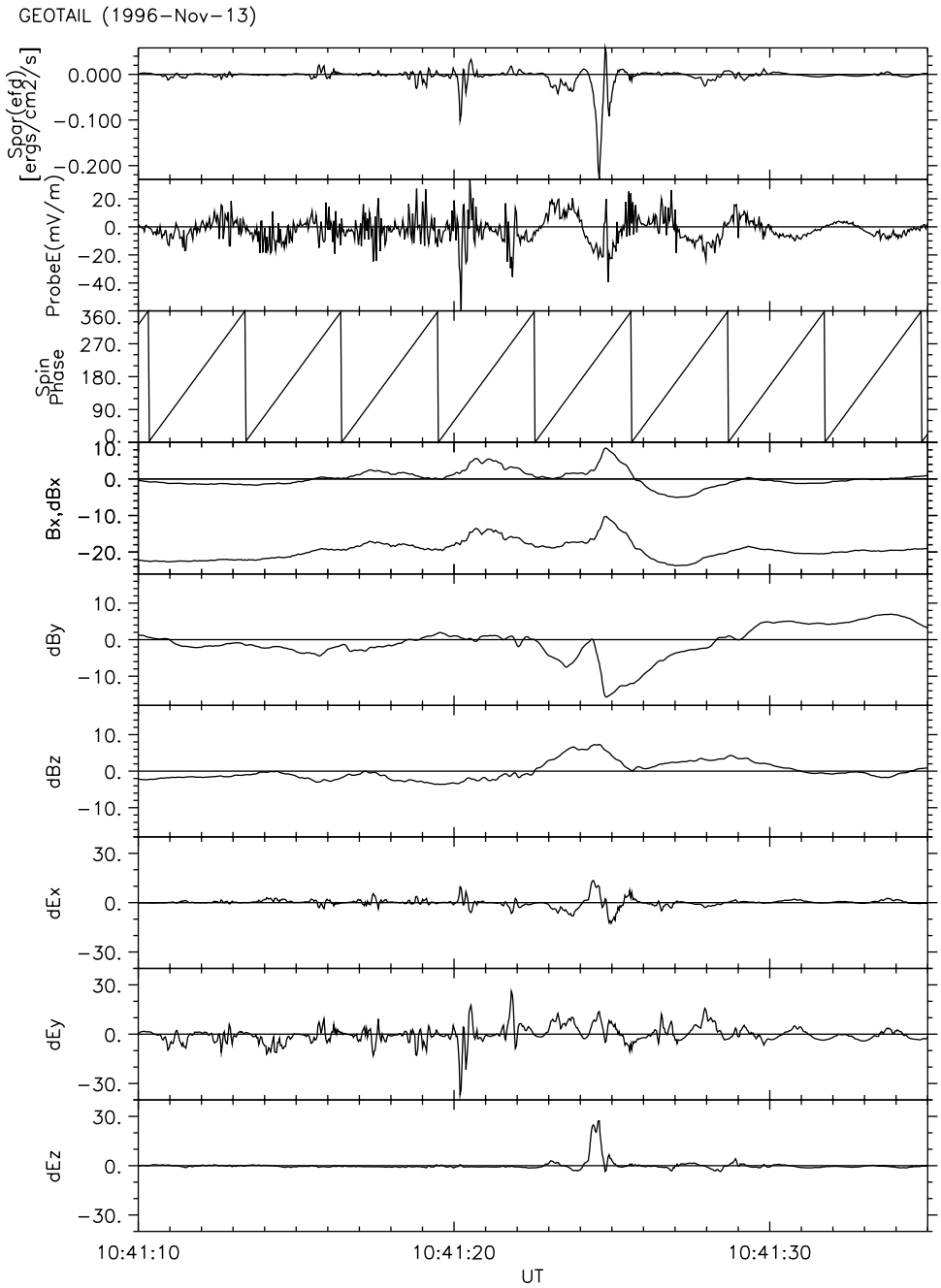

Figure 11. High time resolution electric and magnetic field data from Geotail. SPAR is the parallel Poynting flux. ProbeE is the instantaneous measurement of the electric field along the double-probe boom direction. The spin-phase angle is also shown. The $\mathbf{E}_Z$ electric field component is formed, under favorable magnetic field orientations, by projecting the ProbeE measurement along the x and y directions and using the $\mathbf{E} \cdot \mathbf{B} = 0$ approximation.

infer some information about the value of $\mathbf{E}_Z$ is to look for times when the Z component of the magnetic field is a large fraction of the total field (the larger the fraction, the higher the confidence on the inferred $\mathbf{E}_Z$ value). At such times we can obtain a better estimate of the $\mathbf{E}_Z$ component by using the projections of the antenna measurement on the X and Y axes and the $\mathbf{E} \cdot \mathbf{B} = 0$ approximation. Although kinetic low-frequency waves, such as kinetic Alfven waves, would have a finite parallel electric field component, this would be very small relative to the other components. Since we are mostly interested in obtaining the north-south component and the related Poynting flux, we will ignore the parallel component and use $\mathbf{E} \cdot \mathbf{B} = 0$ to obtain the third component under fortuitous magnetic field geometries. (In any case, the presence of a parallel component does not enter the computation of the Poynting flux.)

[30] Such was the case (only for a short period during the event considered) at ~1041:24 UT. The interval is shown in Figure 11. The electric and magnetic field data have been detrended (high-pass filtered) by subtracting a 20-s-window

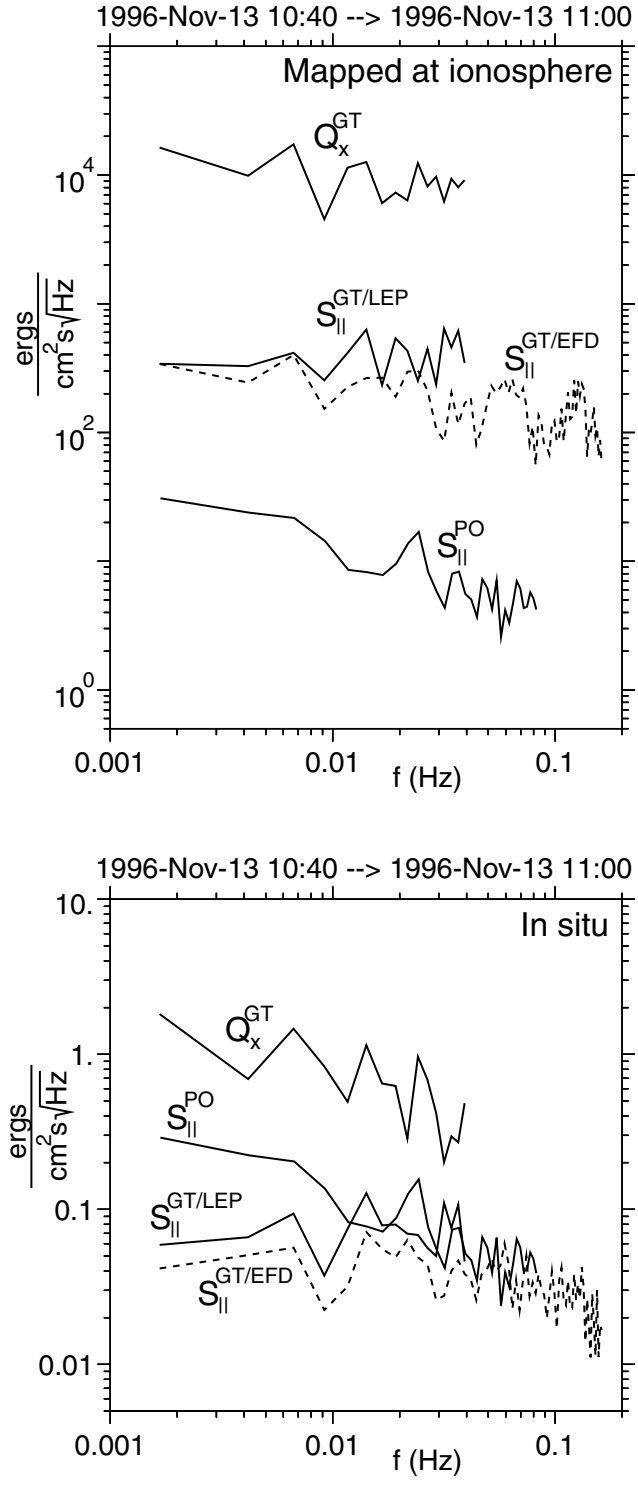

Figure 12. Spectral density of Poynting flux on Polar and Geotail and energy flux on Geotail mapped (top) at 100 km altitude and (bottom) from in situ measurements.

running average, and then they were running averaged at 0.1 resolution. These band-pass-filtered data are shown as d**E** and d**B** quantities. Also shown in the d$\mathbf{B}_X$ panel is the X component of the magnetic field, $\mathbf{B}_X$, for reference. The spin-phase angle between the boom and the X axis is also shown. The electric field data show spikes on the order of 10 s of mV m^{-1} (occasionally these spikes exceed the maximum digitization level of the instrument of 70 mV m^{-1}), and those spikes correspond to peaks in the Poynting flux. However, at ~1041:24 UT a partial entry near the plasma sheet (evidenced by a decrease in the value of $\mathbf{B}_X$) permitted computation of the third component ($\mathbf{E}_Z$) from the projection of the boom-aligned electric field measurement on the X and Y axes. This results in a peak in d$\mathbf{E}_Z$ and the resultant Poynting flux at a value of 0.23 ergs cm^{-2} s^{-1} directed toward the ionosphere. When mapped to an altitude of 100 km (mapping factor of 50,000/18 nT = 2780), we obtain a value of 640 ergs cm^{-2} s^{-1}, which exceeds the values obtained from mapping high-frequency Polar Poynting fluxes by a factor of 3. Since the Geotail measurements are a lower limit of the true Poynting flux values, our conclusion is that the high-frequency spectrum (up to 0.1-s resolution) of the Poynting flux at Geotail also shows the same trend as the lower frequency spectrum, i.e, that its ionospheric projection is several times larger than values obtained nearly simultaneously on Polar.

[31] We now turn to the particle energy flux measured at Geotail. This is the energy flux Q and includes the kinetic energy flux, thermal energy flux, and magnetic energy flux. The dominant term is the thermal energy flux, since in a high-beta plasma both the flow speed and the Alfven speed are smaller than the thermal speed. Since in bursty bulk flows the preferential direction of motion is the X direction, Q_X will dominate over the other components. In Figure 11 (top panel) we present Q_X in ergs cm^{-2} s^{-1}. This ought to be compared with the local measurements of the Poynting flux at the same time resolution (12 s) as obtained from the plasma instrument; it is evident that the peaks in the particle energy flux are 1 order of magnitude larger than the peaks in the Poynting flux. This suggests that if only a small fraction of the equatorial particle energy flux is converted to electromagnetic energy in the form of propagating Alfven waves along the boundary, then it is sufficient to account for the locally measured Poynting flux. In fact, it is reasonable to expect that a significant fraction of the BBF energy will indeed couple to adjacent plasma sheet regions and will radiate Alfven waves along the plasma sheet boundary. If an average magnetic field of 15 nT is used for purposes of mapping to 100 km altitude, the peak earthward energy flux would correspond to 2000 ergs cm^{-2} s^{-1}, although both the field value used for the mapping and the low time resolution of the measurement (12 s) suggest that the mapped value is probably an underestimate.

[32] The above relationship of energy budgets along the auroral flux tubes during substorms is not confined to the short-lived peaks in the Poynting flux, but rather persists in all frequency ranges, as evidenced in Figure 12. Shown in the bottom panel of Figure 12 is the spectrum of the energy flux (the square root of the power spectral density) in units of energy flux per root Hz. When mapped to a common altitude (100 km) at the ionosphere, the energy flux spectra from the different satellites can be readily compared. This is done in the top panel of Figure 12. It is evident there that in all frequencies the Poynting flux measured at Polar is an order of magnitude smaller than the Poynting flux measured at Geotail. It is also evident that in all frequency ranges the particle energy flux measured locally at Geotail is 1 order of magnitude larger than the Poynting flux measured on the

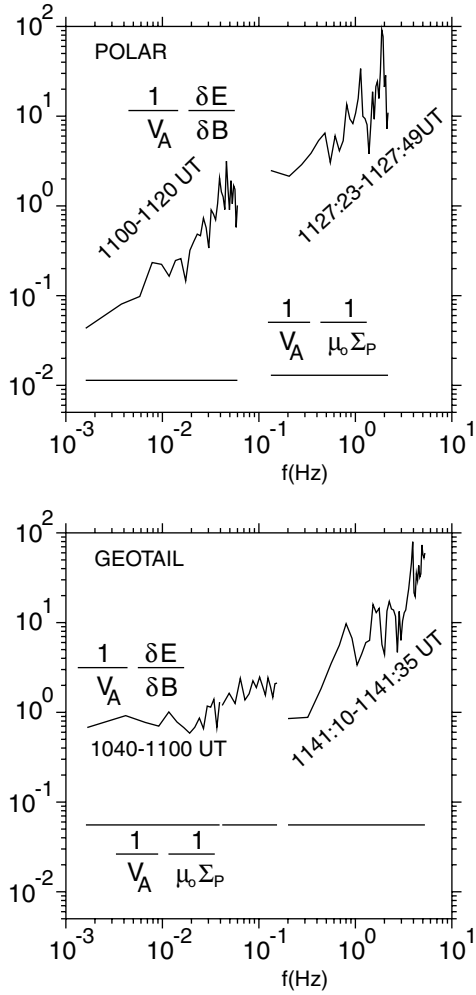

Figure 13. **E**-to-**B** ratios normalized to the local Alfven velocity and plotted as a function of frequency. Also shown are the values of inverse of a nominal height integrated Pedersen conductivity of Σ_P = 10 mhos.

same satellite. These results are only weakly dependent on the interval selected within this active period. In fact, the fluctuation amplitudes of plasma and field data measured at Geotail are typical of BBFs, and the peak energy flux values (for both SPAR and for Q_X) are expected during most BBF intervals. Moreover, the results obtained from spectral comparisons of the energy flux hold when the most active 20-min interval at Geotail is compared with the most active (though different) 20-min interval at Polar during the same substorm event.

4. E-to-B Ratios

[33] In an effort to understand whether the waves are propagating Alfvenic waves or spatial structures closing through the ionosphere, we plot in Figure 13 the ratio of **E** over **B** versus frequency for both spacecraft. The plots are normalized to the local Alfven speed. In the case of Geotail we used the $\mathbf{E}_Z$ component inferred from the plasma flow at frequencies below 1/24 Hz and the $\mathbf{B}_Y$ component at the same (12-s) resolution. The $\mathbf{E}_Y$ and $\mathbf{B}_Z$ components were used between 1/24 and 1/6 Hz (at 3-s resolution) after checking that at lower frequencies the $\mathbf{E}_Y/\mathbf{B}_Z$ ratio was equal to or somewhat larger than the $\mathbf{E}_Z/\mathbf{B}_Y$ ratio. The Y_{GSM} projection of the electric field measured along the double-probe axis and the measured $\mathbf{B}_Z$ were used for frequencies higher than 1/6 Hz, up to 10 Hz (signal-to-noise ratio from fluxgate magnetometer is significantly reduced above 10 Hz). In the case of Polar the ratio of power in the $\mathbf{E}_Z$ and $\mathbf{B}_{56}$ components was used at all frequencies. The high-frequency time intervals were chosen to correspond to the time series of Figures 9 and 11. The low-frequency time intervals were chosen here to be continuous 20-min plasma sheet intervals at times of increased wave activity.

[34] Also plotted for each frequency regime in Figure 13 is the inverse of the nominal, height-integrated Pedersen conductivity, Σ_P = 10 mhos, anticipated at the auroral ionosphere. Spatial structures closing through the ionosphere are expected to have $\delta\mathbf{E}/\delta\mathbf{B}$ ratios that are equal to $1/\mu_0\Sigma_P$.

[35] On Geotail it is evident both in the frequency-dependent **E**-to-**B** ratios of Figure 13 and also by simply taking the ratio of the perturbation amplitudes of $d\mathbf{E}_Z$ ($\sim$30 mV m^{-1}) and $d\mathbf{B}_Y$ ($\sim$10 nT) during the 1041:24.5 UT Poynting flux spike in Figure 11, that the **E**-to-**B** ratio is $\sim$3000 km s^{-1}, which is twice the local Alfven velocity ($\sim$1400 km s^{-1}). Thus, if the structures that are responsible for the peak Poynting flux at Geotail are indeed Alfven waves, then they are likely in the kinetic regime.

[36] On Polar, structures below 0.05 Hz are consistent with spatial structures, especially if lower values of Pedersen conductivity are used ($\sim$1–5 mhos). Fluctuations at frequencies between 0.05 and 1 Hz are consistent with Alfvenic structures, whereas higher-frequency fluctuations may be, at least partly, electrostatic waves. Some of those waves are evident in the $d\mathbf{E}_Z$ component in Figure 9 as $\sim$1-s-period and $\sim$0.15-s-period waves, modulating the large-amplitude electric field structure. However, the rise-and-fall time of the large electric field structure associated with the Poynting flux peak is $\sim$5 s, and the **E**-to-**B** ratio in the associated frequency range (0.2 Hz) is near the Alfven velocity. As evidenced by taking the ratio of the electric to magnetic perturbations near the Poynting flux of Figure 9, $\delta\mathbf{E}/\delta\mathbf{B} \approx$ (150 mV m^{-1})/10 nT $\approx$ 15,000 km s^{-1}, which is $\sim$2.5 times the local Alfven speed ($\sim$6150 km s^{-1}). Thus, if the above structure, which is associated with the peak value in Poynting flux, is Alfvenic, it is also, quite likely, kinetic.

5. Ionospheric Projection

[37] Figure 14 shows the ion and electron differential energy flux spectra during the last part of the Polar plasma sheet crossing, encompassing the interval plotted in Figure 9. It is evident that during the crossing of the outermost L shells of the plasma sheet, upflowing ion bursts of energies 0.5–10 keV were seen at Polar. In the same period, field-aligned electrons (into or out of the ionosphere) at energies 0.05–2 keV are evident. At the time of the large Poynting flux spike plotted in Figure 9, one of the largest energy and intensity upflowing ion beams was seen (marked by the vertical arrow above the top panel and below the bottom panel in Figure 14). The differential energy fluxes of downgoing and upgoing electrons are shown in Figure 15.

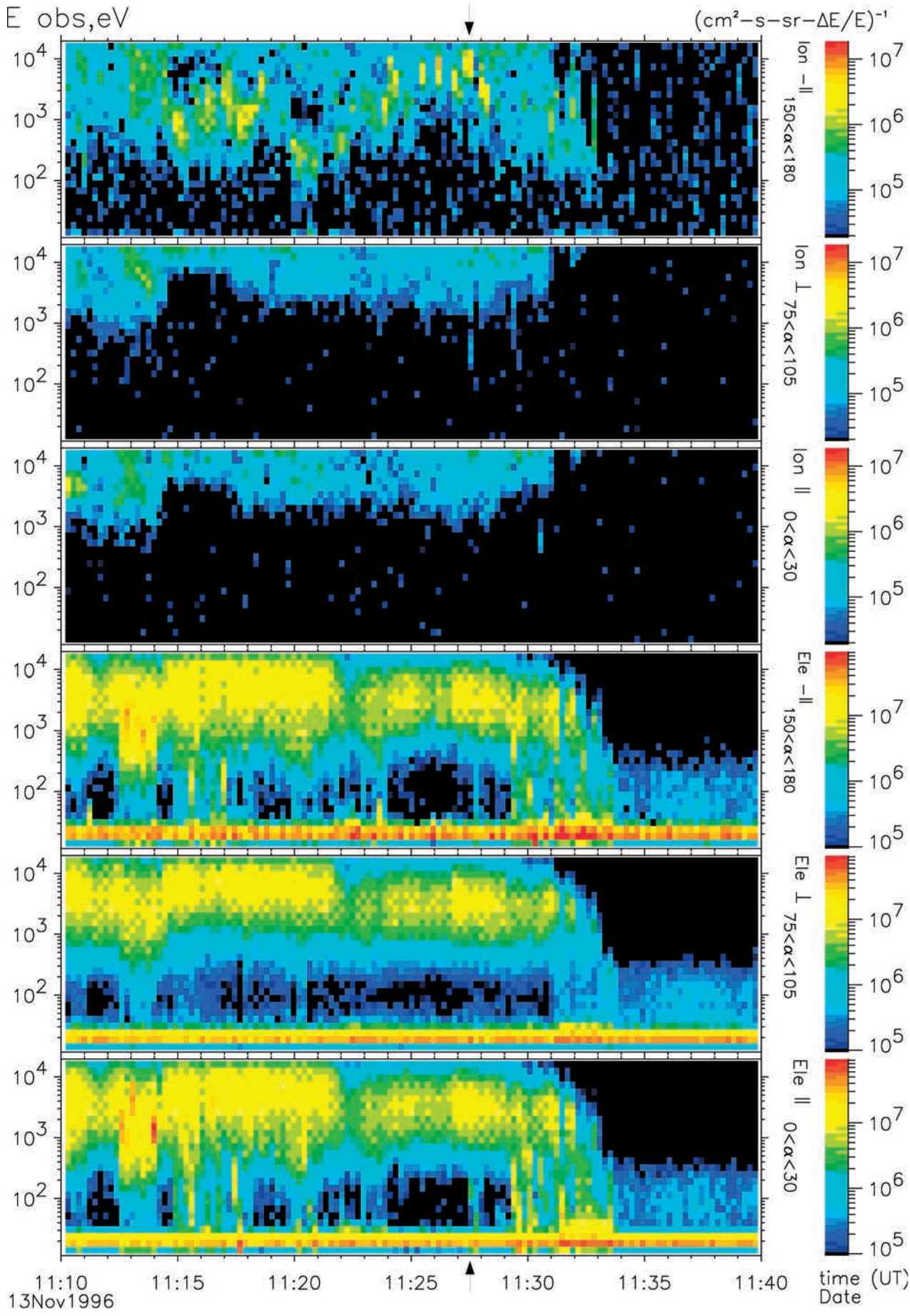
E obs,eV
(cm²−s−sr−ΔE/E)⁻¹
Ion −||
150<α<180
Ion ⊥
75<α<105
Ion ||
0<α<30
Ele −||
150<α<180
Ele ⊥
75<α<105
Ele ||
0<α<30
10⁴
10³
10²
10⁷
10⁶
10⁵
11:10
13Nov1996
11:15
11:20
11:25
11:30
11:35
11:40
time (UT)
Date

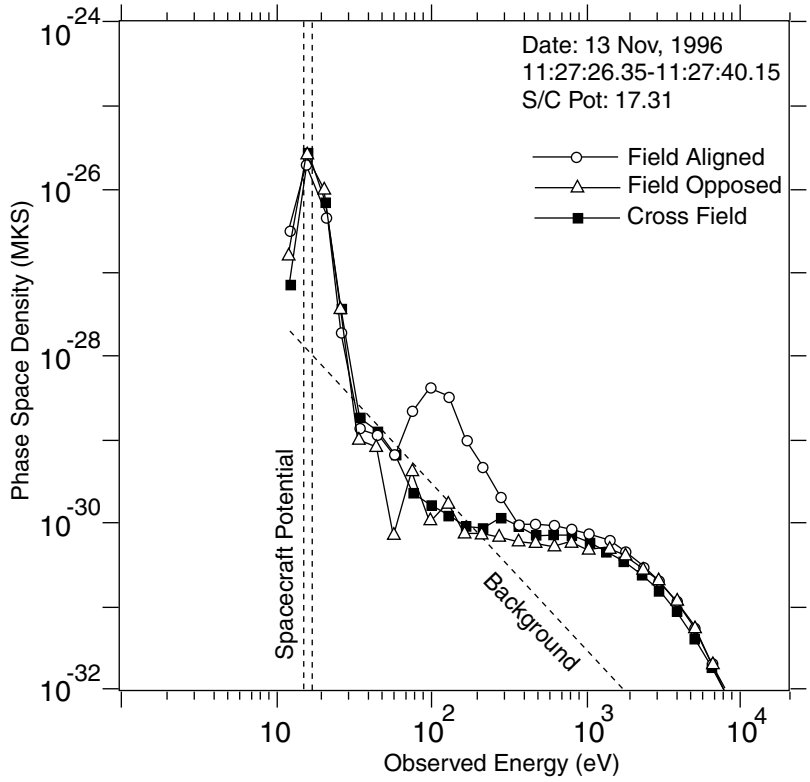

Figure 15. Cuts through the parallel and antiparallel electron distributions in units of phase space density (s^3 m^{-6}) at the time of observation of the large Poynting flux spike on Polar, demarcated by arrows in Figure 14.

The downgoing electrons of energy ~0.05–2 keV dominate over the upgoing electrons of the same energy. The opposite scenario occurs at other instances. The observation of upflowing ions and counterstreaming electron beams at the times of the peak Poynting flux at Polar also helps identify the region in the ionosphere where Polar maps. According to Fast Auroral Snapshot (FAST) observations [*Carlson et al.*, 2000], these are features characteristic of particle populations poleward of the inverted-V region. This region (nightside oval poleward of the aurora) is responsible for some of the largest ion outflows seen around the oval. The electron acceleration there can occur as a result of the acceleration of plasma sheet electrons by Alfven waves [*Chaston et al.*, 2000], which are in the inertial regime [*Lysak and Lotko*, 1996].

[38] Figure 16 shows the Geotail electron distribution on the *X*-*Y* plane (in spacecraft coordinates, which are close to GSE) at two times prior to (but near) the observation of the large Poynting flux spike of Figure 11. The line plots to the right of the polar plot are the distribution function velocity spectra, with the red line representing the spectrum along the red mark on the polar plot (sector 13, near-antisunward direction, i.e., parallel to the field) and with the green line representing the spectrum in the opposite direction (near-sunward direction, parallel to the field). One full Geotail distribution is measured once per spin (3 s); distributions are averaged on board for four spins. The distribution during the 12 s encompassing the time of the spike is not available, but the distribution prior to it is the one presented at the bottom of Figure 16. It is evident that the electron distribution is anisotropic. Similar anisotropic electron distributions are observed throughout this active period and in other Geotail observations of fast flows. The details of the distribution shown at the bottom of Figure 16, i.e., low-energy electrons (below 1 keV) being mostly toward the Earth and high-energy electrons (above 1 keV) being mostly toward the tail, are not to be trusted because of temporal aliasing. But the low-energy bidirectional anisotropy is present, on-and-off, throughout the event, with either the field-aligned or the field-opposed direction having larger fluxes. For example, the distribution shown at the top of Figure 16 was taken ~1 min earlier than that at the bottom of Figure 16, with one (less anisotropic) distribution available in between. The spacecraft potential, as measured by Geotail/EFD, was on the order of 40 eV or less at that time, and energies affected by photoelectron contamination have been removed from the plot presented. The important thing here is that low-energy electrons (~100 eV) show a field-aligned anisotropy in the earthward direction in the top distribution

Figure 14. (opposite) Ion and electron energy flux spectrograms from the HYDRA instrument on the Polar satellite. Arrows mark the times of peak Poynting flux observation. Data are arranged in pitch angle ranges of 0–30, 75–105, and 150–180 degrees, as indicated by color bars. Top three panels are electrons and bottom three panels are ions.

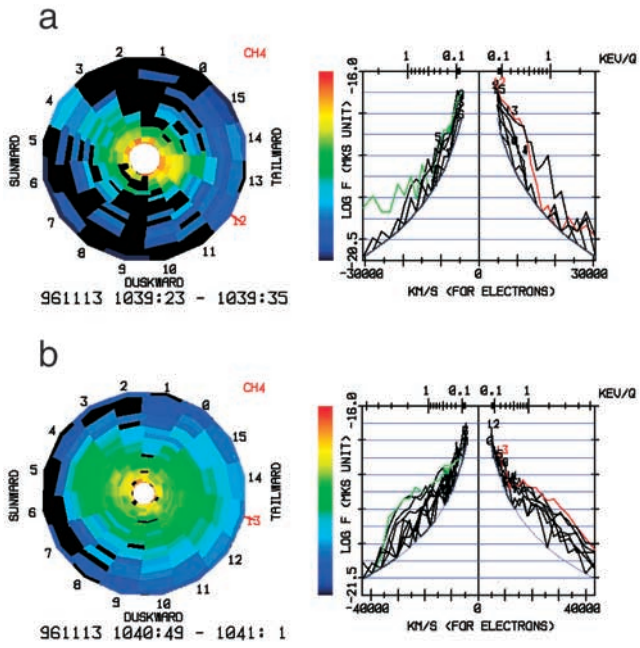

Figure 16. Electron distributions from the LEP instrument on the Geotail satellite for two times near the observation of the large Poynting flux spike of Figure 11.

while the same energy electrons have a tailward anisotropy in the bottom distribution.

[39] The transient, anisotropic nature of the low-energy electron distributions suggests that bidirectional electron beams may be present at timescales that are not resolved by the accumulation rate of the plasma instruments on Geotail and Polar (shorter than 6 s). The parallel flux of the 100-eV electrons at Geotail is $\sim 10^{-17}$ s^3 m^{-6}, which is similar to that observed at Polar in the same energy range (Figure 17). This further reinforces our earlier conjecture that Polar and Geotail were along flux tubes that undergo similar processes, i.e., flux tubes that connect to the region poleward of the auroral arcs.

[40] The presence of copious amounts of electromagnetic energy radiated from the altitude of Geotail toward the ionosphere suggests that the ultimate source of the energy that accelerates the electrons and ions is most likely the bursty bulk flows and that the energy propagates toward Earth in the form of Alfven waves.

6. Conclusions

[41] Comparisons of the field-aligned Poynting flux at Polar and at Geotail, after accounting for mapping along flux tubes to the same reference altitude of 100 km, show that in all frequency ranges between 1 mHz and 0.1 Hz the electromagnetic energy generated at Geotail exceeds the one measured at Polar by a factor of 10. This situation continues beyond 0.1 Hz, where peak Poynting fluxes measured at Geotail exceed those measured at Polar by at least a factor of 3. This suggests that significant energy dissipation takes place along auroral field lines and before it reaches Polar.

[42] Our comparisons of the peak Poynting flux measured at Polar during this substorm event with typical Poynting fluxes expected on auroral field lines below the acceleration region suggest that the peak Poynting flux at high time (1/40 s) resolution exceeds that anticipated by in situ ionospheric measurements by a factor of 100. The amount of energy flux measured at Polar is comparable to the largest energy fluxes observed in the precipitating electrons (plus upflowing ions and secondary electrons) during substorm times.

[43] At frequencies below 0.05 Hz, **E**-to-**B** ratios on Geotail are consistent with Alfvenic oscillations, whereas on Polar they are below the Alfven speed. For low values of the ionospheric conductivity, low-frequency waves on Polar are consistent with current filaments closing through the ionosphere. At frequencies of $\sim$0.05–1 Hz, where the largest Poynting flux peaks are observed at both spacecraft, the **E**-to-**B** ratios at Geotail are many times larger than the local Alfven speed and are consistent with kinetic Alfven waves, whereas at Polar they are in the Alfvenic regime. The parallel electric field associated with the Polar peak Poynting fluxes is below the uncertainty arising from spin vector knowledge inaccuracies and instrument offsets ($\sim$1 mV m^{-1}).

[44] The presence of increased field-aligned electron fluxes near the times of peak Poynting flux on both spacecraft reinforces our conjecture that the two spacecraft map along field lines that undergo similar processes. The observation of peak flux and peak energy upflowing ions on Polar near the times of the anisotropic electrons and the

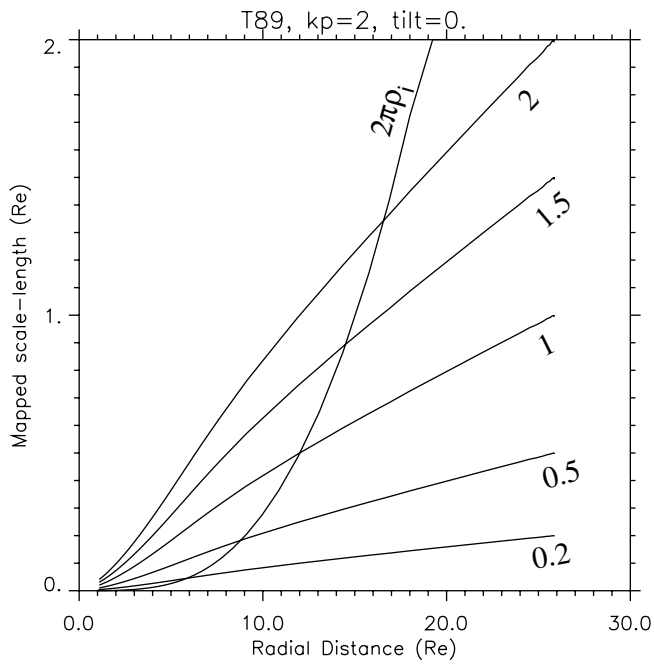

Figure 17. Plots of the cross-scale size of a flow burst mapped along a realistic magnetic field model (T89) from the equatorial magnetotail down to the ionosphere. Different values denote a different starting spatial scale in units of R_E. Also shown is the quantity $2\pi\rho_i$, assuming a constant ion temperature of 4 keV as ex-pected from Liouville mapping. At a given radial distance, kinetic effects start becoming important when $2\pi\rho_i/d \geq 0.2$, where d is the mapped flow burst size. For a 1-R_E equatorial cross-tail-size flow burst, this corresponds to an altitude of 6 R_E.

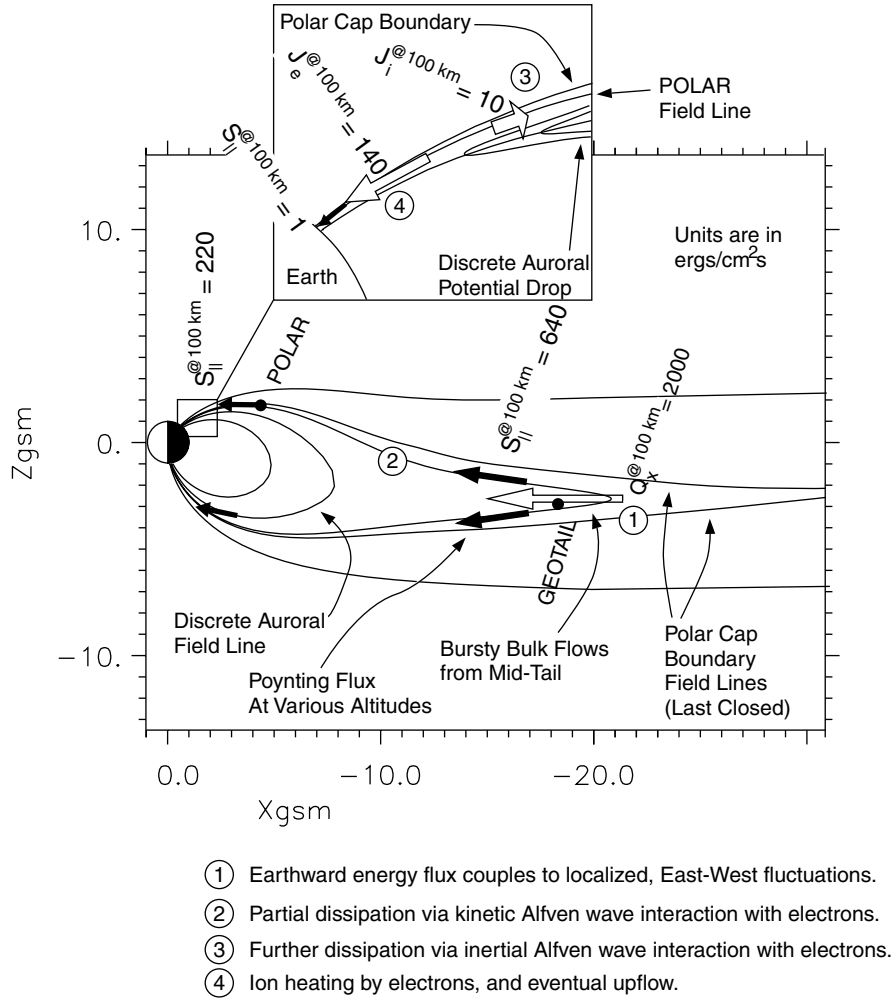

Figure 18. Schematic representation of process of energy generation and dissipation along field lines. Peak energy fluxes measured and particle fluxes expected at low altitudes are also shown. All energy flux values are in units of ergs cm^{-2} s^{-1} and have been mapped to an altitude of 100 km. Low-altitude observations are not made in this paper but are maximum total values inferred from observations on other platforms (see section 3 for references to those sources).

peak Poynting fluxes suggests that the region where both spacecraft map is just poleward of the parallel potential associated with the auroral structures. Figure 18 summarizes our observations and associates them with particle and pointing flux observations at low altitudes.

7. Discussion

7.1. On the Generation of V_y Flows

[45] It is remarkable that despite the dominance of the $\mathbf{V}_X$ flows (and the secondary nature of the $\mathbf{V}_Y$ flows) in terms of energy transport, the $\mathbf{V}_Y$ flows measured at Geotail appear to dominate in terms of their contribution to the Poynting flux out of the plasma sheet and into the auroral ionosphere. This situation may be even more pronounced at higher frequencies, where peak Poynting fluxes due to $\mathbf{E}_Z$ fluctuations are inferred at Geotail. In retrospect, this should have been anticipated, since the $\mathbf{V}_X$ fluctuations ($\mathbf{E}_Y$ fluctuation electric fields) are heavily damped because of the coupling between the Alfven and the slow mode, arising from the field-line curvature [*Southwood and Saunders*, 1985].

[46] The generation of $\mathbf{V}_Y$ fluctuations in connection with bursty flows is difficult to ascertain without multiple satellites. However, it is reasonable to expect that the interaction of localized earthward jets of plasma with the preexisting (relatively slow or stationary) plasma sheet plasma would drive significant east-west plasma motion. Such is the case in observations by *Sergeev et al.* [1996] of localized bursty flow structures, therein termed "bubbles" in reference with the theoretical model of *Chen and Wolf* [1993]. These authors used two satellites to study the properties of the incoming flow when the magnetic field had a sharp boundary that permitted usage of the minimum variance technique to determine the satellite location relative to the east-west center of the structure. It was found not only that the flow deflected dawnward when the satellite was located duskward of the flow center (and vice versa on the other side) but also that the magnetic field was deflected consistently, i.e., by the correct sign expected if the field lines were swept sideways along with the flow. Multiple localized flow bursts, which are common within BBFs, can naturally cause

considerable $\mathbf{V}_Y$ fluctuations and a resultant large, fluctuating $\mathbf{E}_Z$ field.

[47] An alternative (and most likely comanifest) process that ought to result in large Poynting fluxes is the process of magnetotail reconnection. Since the reconnection process in the tail is transient and localized [e.g., *Angelopoulos et al.*, 1996b], we expect that the ionospheric area mapping directly to the reconnection site(s) is limited relative to the area affected by the resultant flows and their shear.

7.2. On Mapping

[48] An exact mapping along field lines is rather difficult to obtain over large distances. In addition, multiple, localized acceleration sites can also result in incoherent signatures on the two satellites, even when the equatorial footprints are within a few R_E in Y of each other. In this paper we resorted to comparing Poynting flux increases observed at different times but during the same phase of the substorm (recovery phase). In fact, the event chosen represents the most viable candidate for comparison because of the similarity of the features on the two spacecraft (large variability in fields and encounters of similar plasma regions) and because of the substorm that was taking place simultaneously. The times of observation are probably related to spatial motions of the active region past the satellites rather than to temporal intensifications. The peak Poynting fluxes at the two satellites are then the most relevant quantities to compare. Supporting evidence of our mapping along flux tubes undergoing similar processes is the observation of bidirectional electron streaming on both spacecraft at or near the time of observation of peak Poynting flux.

[49] One might still argue that since the Polar and Geotail Poynting flux "spikes" occur at different times, they may represent different magnitude intensifications, and therefore they cannot be readily compared. However, the properties of the electric field and Poynting flux on Polar are typical of most active time crossings of the plasma sheet boundary by Polar [*Wygant et al.*, 2000], while the properties of the plasma, electric field, and Poynting flux at Geotail are typical of BBFs [*Angelopoulos et al.*, 1994]. Thus, although the peak Poynting fluxes that are compared may not be along the same flux tubes, they are typical of the regions traversed by Polar and Geotail at substorm recovery. The event studied, selected among many candidates because of the similarity of the features on both satellites during the course of a substorm, epitomizes what in retrospect seems obvious by event studies on the individual satellites: There is plenty more Poynting flux escaping from the tail than is measured at 5–6 R_E above auroral field lines, by a factor of $\sim$10.

7.3. On Energy Dissipation

[50] It is possible that energy loss is due to partial reflection along field line. To evaluate this, we considered the relative change of the Alfven conductivity per unit wave travel time in a realistic magnetic topology (T89 model). We found that this quantity differs only slightly from its value in a dipole geometry [*Mallinckrodt and Carlson*, 1978] and is very close to zero compared to its value at low altitudes (<4 R_E). This suggests that waves cannot really be reflected between Polar and Geotail. Another argument against partial reflection is that reflected waves would be broadened and would have resulted in large upward moving Poynting flux, something that is not observed here.

[51] Alternative explanations for the energy loss are dissipation along field line or escape of wave power across field lines, both of which require the presence of dispersive Alfven waves. Kinetic Alfven waves were proposed initially by *Hasegawa and Chen* [1975] to explain heating of electrons and ions at a resonant layer on magnetospheric (and tokamak) field lines by a surface wave at the magnetopause (driver). The concept is that when the incoming compressional oscillations reach the resonant layer, they become kinetic, now propagating across the magnetic field because of the finite perpendicular wavelength supported by the finite ion gyroradius and/or the finite electron inertia. In the collisionless regime the parallel electric field of the kinetic Alfven wave interacts with and heats primarily the electrons. The possibility of the existence of kinetic Alfven waves at the plasma sheet boundary was utilized in the thermal catastrophe model of substorms [*Goertz and Smith*, 1989] in which the incoming waves were plasma sheet boundary layer surface waves and the kinetic Alfven waves were excited through mode conversion of these compressional surface waves. The presence of a magnetic field and plasma pressure gradient at the boundary layer was the reason for mode conversion of the incoming waves.

[52] The kinetic Alfven waves (which are operational in the regime $m_e/m_i < \beta_e < 1$) and their distinction from the inertial Alfven waves (which depend on finite electron inertia and are operational in the regime $\beta_e < m_e/m_i$) were recently discussed by *Lysak and Lotko* [1996]. By using typical plasma sheet electron temperatures (0.5 keV) and densities (0.2 cm^{-3}) and a realistic magnetic field model (T89), it is possible to show that regions above 5 R_E have an electron beta between m_e/m_i and 1. The electron beta exceeds 1 either near the plasma sheet boundary at distances beyond $\sim$18 R_E when the Alfven speed decreases considerably or as soon as the field line penetrates very deeply near the neutral sheet, i.e., when the ion beta is >7 for a typical $T_i/T_e \approx 7$ [*Baumjohann et al.*, 1989]. In our case, the entire region between Geotail and Polar (except for the layer near the center of the plasma sheet of beta >7) can support kinetic Alfven waves of the regime discussed by *Hasegawa and Chen* [1975] and *Lysak and Lotko* [1996]. Since there is ample power in the bursty bulk flows to generate the Poynting fluxes observed along auroral/plasma sheet field lines, there is no need to invoke an external global-mode oscillation for generating kinetic Alfven waves, as was done by the earlier authors. Instead, the waves will be kinetic if the driver has perpendicular scale lengths λ comparable to $2\pi\rho_i$. For layers adjacent to the neutral sheet ($\mathbf{B} \sim 10$ nT, $T \sim 4$ keV), this value is $2\pi\rho_i \approx 1\ R_E$. This is within the range of anticipated cross-scale size of BBFs [e.g., *Angelopoulos et al.*, 1997].

[53] More precisely, when the T89 mapping is used to map a BBF of an equatorial scale size of $\sim 1 R_E$ (range 0.2–2 R_E is used) along the field lines and to compare that with the ion gyroradius, assuming a 4-keV ion temperature, we obtain the results of Figure 17. For example, for a BBF equatorial scale size of 1.5 R_E, and assuming that finite wavelength effects are important for scale lengths $\geq 2\pi\rho_i$, the Alfven waves will remain kinetic down to at least an

altitude of 15 R_E. In reality, kinetic effects will be important if the mapped scale lengths are only a fraction of $2\pi\rho_i$, e.g., $0.2 \times 2\pi\rho_i$, in which case the critical distance below which such effects will be important for a 1-R_E cross-scale size BBF will be obtained from the crossover of the curve labeled 0.2 with the curve labeled $2\pi\rho_i$. This distance is $\sim$6 R_E, i.e., the Polar altitude. It is thus evident that between Polar and Geotail altitudes the scale size of the bursty flows are in the kinetic Alfven wave regime (i.e., of the order of $2\pi\rho_i$) simply due to the anticipated scale size (or structuredness) of the driver. The parallel electric field associated with such structures may be very small and depends on the perpendicular wavelength of the waves, with longer wavelengths having smaller parallel fields. Thus our observation of a parallel electric field below the 1 mV m^{-1} confidence level on Polar is not inconsistent with kinetic waves.

[54] Since the electrons interacting with the waves are fast and field aligned, we expect parallel heating all along the field line. The heating would stop when the waves are damped, and the parallel anisotropy would then relax through wave-particle interactions or middle-and upper-atmosphere scattering at the equatorial foot of the field line over many electron bounces. Thus we expect an anticorrelation between electrons and Poynting flux spikes. This is a matter of future research, has not been observed thus far to our knowledge, and is not inconsistent with our data: As we observed, counterstreaming electrons are observed in the vicinity of the Poynting flux spikes, but a one-to-one correlation has actually not been noted.

[55] We have computed the integrated electron energy flux measured in the vicinity of the observed Poynting flux spikes ($J_e \approx 10^7$ eV $(cm^2$ s str eV$)^{-1}$). With reasonable assumptions (solid angle of 1/4str and $\Delta\mathbf{E}$ = 300 eV) we get 10^{-3} ergs cm^{-2} s^{-1}. This is 3 orders of magnitude smaller than the measured Poynting flux at Polar. The situation may be similar to low-altitude measurements (e.g., FAST) where temporal resolution (and aliasing) is known to inhibit correct determination of peak field-aligned fluxes. Since the time resolution of Hydra data is 6 s (3-s data have only partial phase space coverage), the field-aligned direction is sampled only once per 6 s, while the peak Poynting flux event duration is only 2 s. On Geotail we have 12-s samples, each of which is, in fact, an average over four consecutive distributions. This temporal aliasing may explain why the expected anticorrelation has thus far not been seen.

[56] Next we estimate the effects of Poynting flux escape along the flux tubes connected to the bursty flows on the flow evolution. This represents a loss term to the incoming earthward particle energy flux. We assume a box geometry in the equatorial plasma sheet. The flow is going earthward and decelerating, while Poynting flux is escaping along field lines. No heating is assumed to occur within the box. Assuming that most of the energy is lost along the field line before it reaches the altitude of Polar (a distance $L \sim 10\ R_E$), we seek the timescale within which the bursty flow will deposit all its energy via Poynting flux. Since most of the particle energy flux is in the term $V_X \times P$ [*Angelopoulos et al.*, 1994], the rate of change of the particle energy is $\Delta V_X \times P_i/\Delta X$ while the rate of change of electromagnetic energy is $\Delta S/L$ times a factor of 2 for the northern and southern ionosphere. Equating the two, we obtain $\Delta X/\Delta V_X = 0.5 P_i \times L/\Delta S$. This quantity has units of time and represents the timescale for stopping of the BBF due to radiation of electromagnetic energy away from it. Substituting the typical values of the Poynting flux measured at Geotail (0.01 ergs cm^{-2} s^{-1}) and for typical ion pressures (P_i = 0.13 nPa arising from T_i = 4 keV and N_i = 0.3 cm^{-3}) we obtain a timescale of $\sim$10 min. This is close to the observed median BBF duration. If we take peak values of Poynting flux at Geotail (0.1 ergs cm^{-2} s^{-1}), then the stopping time is 10 times faster, i.e, 1 min. The latter is more appropriate for individual flow bursts. In the above calculation the pressure gradient and the change in the magnetic field have been assumed small. Close to Earth these are significant. However, far from Earth, where the tailward gradients are weak, the above calculation suggests that enough power escapes via Poynting flux along the field to account for BBF deceleration.

[57] This can explain why bursty flows far from Earth can be seen without near-Earth flow consequences [*Coroniti et al.*, 1978, 1980; *Oieroset et al.*, 2000] and without any significant auroral electrojet intensifications. Much of their energy can couple through flow shear to dawn-dusk flow components that radiate electromagnetic energy along field lines. Much of that energy couples into electron heating and/or is radiated out of the flux tube. High-latitude filamentary currents that are seen during midtail flow occurrence can be explained as due to currents carried by the remaining portion of the Alfven waves when they propagate to lower altitudes. Dissipation there (below an altitude of 5 R_E) is expected to take place because of the waves' parallel electric field interaction with electrons as those waves become inertial [e.g., *Chaston et al.*, 2000].

[58] The above scenario can also explain why any tentative candidates for an ionospherically reflected pulse from the incoming flow burst in the data are small in amplitude relative to the incoming flow, as mentioned in section 1. The explanation is that because of the kinetic nature of the wave (parallel electric field and finite perpendicular wavelength) most of the energy is deposited through wave-particle interactions and/or is diffused away from the flux tube as the wave travels to the ionosphere prior to its first bounce.

[59] **Acknowledgments.** We wish to thank C. W. Carlson, J. McFadden, and J. Bonnell for useful discussions. This work was supported by NASA contract NAS5-30367.

[60] Hiroshi Matsumoto thanks A. Nishida and another referee for their assistance in evaluating this paper.

References

Angelopoulos, V., The role of impulsive particle acceleration on magnetotail circulation, *ESA SP-389*, 17 pp., Eur. Space Agency, Noordwijk, The Netherlands, 1996.

Angelopoulos, V., W. Baumjohann, C. F. Kennel, F. V. Coroniti, M. G. Kivelson, R. Pellat, R. J. Walker, H. Lühr, and G. Paschmann, Bursty bulk flows in the inner central plasma sheet, *J. Geophys. Res.*, *97*, 4027, 1992.

Angelopoulos, V., C. F. Kennel, F. V. Coroniti, R. Pellat, M. G. Kivelson, R. J. Walker, C. T. Russell, W. Baumjohann, W. C. Feldman, and J. T. Gosling, Statistical characteristics of bursty bulk flow events, *J. Geophys. Res.*, *99*, 21,257, 1994.

Angelopoulos, V., et al., Multipoint analysis of a bursty bulk flow event on April 11, 1985, *J. Geophys. Res.*, *101*, 4967, 1996a.

Angelopoulos, V., et al., Tailward progression of magnetotail acceleration centers: Relationship to substorm current wedge, *J. Geophys. Res.*, *101*, 24,599, 1996b.

Angelopoulos, V., et al., Magnetotail flow bursts: Association to global magnetospheric circulation, relationship to ionospheric activity, and direct evidence for localization, *Geophys. Res. Lett.*, *24*, 2275, 1997.

Angelopoulos, V., et al., On the relationship between bursty flows, current disruption, and substorms, *Geophys. Res. Lett.*, *26*, 2841, 1999.
Baumjohann, W., G. Paschmann, and C. A. Cattrell, Average plasma properties in the central plasma sheet, *J. Geophys. Res.*, *94*, 6597, 1989.
Baumjohann, W., G. Paschmann, and H. Luhr, Characteristics of high-speed ion flows in the plasma sheet, *J. Geophys. Res.*, *95*, 3801, 1990.
Birn, J., et al., Flow braking and the substorm current wedge, *J. Geophys. Res.*, *104*, 19,895, 1999.
Carlson, C. W., et al., Properties of the plasmasheet boundary layer in the aurora, paper presented at 33rd COSPAR Scientific Assembly, Comm. on Space Res., Warsaw, Poland, July 2000.
Chaston, C. C., et al., Alfven waves, density cavities and electron acceleration observed from the FAST spacecraft, *Phys. Scr. T*, *84*, 64, 2000.
Chen, C. X., and R. A. Wolf, Interpretation of high-speed flows in the plasma sheet, *J. Geophys. Res.*, *98*, 21,409, 1993.
Coroniti, F. V., L. A. Frank, R. P. Lepping, F. L. Scarf, and K. L. Ackerson, Plasma flow pulsations in Earth's magnetic tail, *J. Geophys. Res.*, *83*, 2162, 1978.
Coroniti, F. V., L. A. Frank, D. J. Williams, R. P. Lepping, F. L. Scarf, S. M. Krimigis, and G. Gloeckler, Variability of plasma sheet dynamics, *J. Geophys. Res.*, *85*, 2956, 1980.
Elphinstone, R. D., et al., The double oval UV auroral distribution, 1, Implications for the mapping of auroral arcs, *J. Geophys. Res.*, *100*, 12,075, 1995.
Feldstein, Y. I., and G. V. Starkov, Dynamics of auroral belt and polar geomagnetic disturbances, *Planet. Space Sci.*, *15*, 209, 1967.
Ghielmetti, A. G., R. D. Sharp, E. G. Shelley, and R. G. Johnson, Downward flowing ions and evidence for injection of ionospheric ions into the plasma sheet, *J. Geophys. Res.*, *84*, 5781, 1979.
Goertz, C. K., and R. A. Smith, The thermal catastrophe model of substorms, *J. Geophys. Res.*, *94*, 6581, 1989.
Harvey, P., et al., The electric field instrument on the Polar satellite, *Space Sci. Rev.*, *71*, 583, 1995.
Hasegawa, A., and L. Chen, Kinetic process of plasma heating due to Alfven wave excitation, *Phys. Rev. Lett.*, *35*, 370, 1975.
Henderson, M. G., G. D. Reeves, and J. S. Murphree, Are north-south aligned auroral structures an ionospheric manifestation of bursty bulk flows?, *Geophys. Res. Lett.*, *25*, 3737, 1998.
Keiling, A., J. R. Wygant, C. Cattell, M. Temerin, F. S. Mozer, C. A. Kletzing, J. Scudder, C. T. Russell, W. Lotko, and A. V. Streltsov, Large Alfven wave power in the plasma sheet boundary layer during the expansion phase of substorms, *Geophys. Res. Lett.*, *27*, 3169, 2000.
Kelley, M. C., D. J. Knudsen, and J. F. Vickrey, Poynting flux measurements on a satellite: A diagnostic tool for space research, *J. Geophys. Res.*, *96*, 201, 1991.
Kepko, L., and M. G. Kivelson, Generation of Pi2 pulsations by bursty bulk flows, *J. Geophys. Res.*, *104*, 25,021, 1999.
Kettmann, G., and P. Daly, Detailed determination of the orientation and motion of the plasma sheet boundary layer using energetic protons on ISEE 1 and 2: Waves, curves, and flapping, *J. Geophys. Res.*, *93*, 7376, 1988.
Lyons, L. R., T. Nagai, G. T. Blanchard, J. C. Samson, T. Yamamoto, T. Mukai, A. Nishida, and S. Kokubun, Association between Geotail plasma flows and auroral poleward boundary intensifications observed by CANOPUS photometers, *J. Geophys. Res.*, *104*, 4485, 1999.
Lysak, R. L., and W. Lotko, On the kinetic dispersion relation for shear Alfven waves, *J. Geophys. Res.*, *101*, 5085, 1996.
Lysak, R. L., and Y. Song, Dynamics of auroral arc formation during substorms, in *Substorms 4*, edited by S. Kokubun and Y. Kamide, p. 35, Kluwer Acad., Norwell, Mass., 1998.
Mallinckrodt, A. J., and C. W. Carlson, Relations between transverse electric fields and field-aligned currents, *J. Geophys. Res.*, *83*, 1426, 1978.
McFadden, J. P., Y. K. Tung, C. W. Carlson, R. J. Strangeway, E. Moebius, and L. M. Kistler, FAST observations of ion outflows associated with magnetic storms, in *Space Weather*, *Geophys. Monogr. Ser.*, vol. 125, edited by P. Song, pp. 413–421, AGU, Washington, D. C., 2001.
Nagai, T., M. Fujimoto, Y. Saito, S. Machida, T. Terasawa, R. Nakamura, T. Yamamoto, T. Mukai, A. Nishida, and S. Kokubun, Structure and dynamics of magnetic reconnection for substorm onsets with Geotail observations, *J. Geophys. Res.*, *103*, 4419, 1998.
Newell, P.T., Reconsidering the inverted-V particle signature: Relative frequency of large-scale electron acceleration events, *J. Geophys. Res., 105*, *15*, 779, 2000.
Nishida, A., Possible origin of transient dusk-to-dawn electric field in the nightside magnetosphere, *J. Geophys. Res.*, *84*, 3409, 1979.
Oieroset, M., et al., Wind and Geotail observations of high speed flows in the mid-tail and near-Earth plasma sheet and their ionospheric signatures, paper presented at 1st S-RAMP conference, Sci. Comm. on Sol.-Terr. Phys., Sapporo, Japan, October 2000.
Russell, C. T., et al., The GGS/Polar magnetic fields investigation, *Space Sci. Rev.*, *71*, 563, 1995.
Sanchez, E. R., J. D. Kelly, V. Angelopoulos, T. Hughes, and H. Singer, Alfven modulation of the substorm magnetotail transport, *Geophys. Res. Lett.*, *24*, 979, 1997.
Schodel, R., R. Nakamura, W. Baumjohann, and T. Mukai, Rapid flux transport and plasma sheet reconfiguration, *J. Geophys. Res.*, *106*, 8381, 2001.
Sergeev, V. A., V. Angelopoulos, J. T. Gosling, C. A. Cattell, and C. T. Russell, Detection of localized, plasma-depleted flux tubes or bubbles in the midtail plasma sheet, *J. Geophys. Res.*, *101*, 10,817, 1996.
Sergeev, V. A., K. Liou, C.-I. Meng, P. T. Newell, M. Brittnacher, G. Parks, and G. D. Reeves, Development of auroral streamers in association with localized impulsive injections to the inner magnetotail, *Geophys. Res. Lett.*, *26*, 417, 1999.
Sergeev, V. A., et al., Multiple-spacecraft observation of a narrow transient plasma jet in the Earth's plasma sheet, *Geophys. Res. Lett.*, *27*, 851, 2000.
Shiokawa, K., W. Baumjohann, and G. Haerendel, Braking of high-speed flows in the near-Earth tail, *Geophys. Res. Lett.*, *24*, 1179, 1997.
Shiokawa, K., G. Haerendel, and W. Baumjohann, Azimuthal pressure gradient as driving force of substorm currents, *Geophys. Res. Lett.*, *25*, 959, 1998.
Southwood, D. J., and M. A. Saunders, Curvature coupling of slow and Alfven MHD waves in a magnetotail field configuration, *Planet. Space Sci.*, *33*, 127, 1985.
Starkov, G. V., Statistical dependencies among indices of geomagnetic activity, *Geomagn. Aeron.*, *34*, 129, 1994.
Stenbaek-Nielsen, H. C., T. J. Hallinan, D. L. Osborne, J. Kimball, C. Chaston, J. McFadden, G. Delory, M. Temerin, and C. W. Carlson, Aircraft observations conjugate to FAST: Auroral arc thicknesses, *Geophys. Res. Lett.*, *25*, 2073, 1998.
Tsyganenko, N., A magnetospheric magnetic field model with a warped tail current sheet, *Planet. Space Sci.*, *37*, 5, 1989.
Wygant, J. R., et al., Polar spacecraft based comparisons of intense electric fields and Poynting flux near and within the plasma sheet-tail lobe boundary to UVI images: An energy source for the aurora, *J. Geophys. Res.*, *105*, 18,675, 2000.
Zesta, E., L. R. Lyons, and E. Donovan, The auroral signature of earthward flow bursts observed in the magnetotail, *Geophys. Res. Lett.*, *27*, 3241, 2000.

V. Angelopoulos, J. A. Chapman, and F. S. Mozer, Space Sciences Laboratory, University of California, Grizzly Peak Boulevard at Centennial Drive, Berkeley, CA 94720-7450, USA. (vassilis@ssl.Berkeley.edu; jchapman@uclink4.berkeley.edu; mozer@sunspot.ssl.berkeley.edu)

T. J. Hughes, Herzberg Institute of Astrophysics, National Research Council, Ottawa, Ontario K1A 0R6, Canada. (terry_hughes@xoommail.com)

T. Mukai and K. Tsuruda, Institute of Space and Astronautical Science, 3 1 1 Yoshinodai, Sagamihara, Kanagawa 229, Japan. (mukai@mukai-v.lcl.stp.isas.ac.jp; tsuruda@gtl.isas.ac.jp)

J. D. Scudder, Department of Physics and Astronomy, University of Iowa, Iowa City, IA 52242, USA. (jds@space-theory.physics.uiowa.edu)

K. Yumoto, Department of Earth and Planetary Sciences, Faculty of Sciences 33, Kyushu University, 6-10-1 Hakozaki, Higashiku, Fukuoka 812-81, Japan. (yumoto@geo.kyushu-u.ac.jp)